# LIGHTWEIGHT CEMENT-FREE ALKALI-ACTIVATED SLAG PLASTER FOR THE STRUCTURAL RETROFIT AND ENERGY UPGRADING OF POOR QUALITY MASONRY WALLS

L. Coppola[1,2], D. Coffetti[1,2], E. Crotti[1,2], A. Marini[1], C. Passoni[1], T. Pastore[1]

[1] Department of Engineering and Applied Sciences, University of Bergamo (Italy)

[2] INSTM, UdR "Materials and Corrosion", Florence (Italy)

**ABSTRACT**

The paper deals with the development of an innovative Portland-free lightweight structural plaster to improve the seismic performance and the energy efficiency of poor quality stone masonry buildings. In particular, one-part alkali-activated slag-based mortars were manufactured with different lightweight glass aggregate contents to be mechanically compatible with historic stone walls (28-day compressive strength up to 8 MPa) and to serve as a thermo-insulating layer (specific mass lower than 1000 kg/m$^3$). Results indicate that the Portland-free alkali activated-based plaster manufactured with expanded glass aggregates and air entraining agent is able to provide a 28-day compressive strength equal to 8 MPa and a thermal conductivity of 0.35 W/mK due to density close to 700 kg/m$^3$. Moreover, by using methylcellulose (MC), modified starch (MS), polypropylene fibers, shrinkage reducing admixture (SRA) and silane-based surface treatment, it is possible to ensure an excellent adhesion to the substrate, the absence of micro-cracks and detachments and a very low water absorption coefficient.

**KEYWORDS**

Alkali-activated slag; Expanded glass; Glass mesh; Reinforced plaster; Seismic improvement; Energy upgrade.

## 1. INTRODUCTION

The growing attention to the preservation of the historical heritage has remarkably boosted research in the field of the structural rehabilitation, drawing the scientific community toward the investigation of the conservation state and the mechanical properties of the materials [1–3], the modelling and the analysis of the structural response of unreinforced and reinforced masonry constructions [4–7], as well as toward the conceptual design of effective and targeted strengthening techniques [8–11]. The vulnerability of the existing historical masonry constructions under static and dynamic loads was repeatedly observed, particularly in the aftermath of recent Italian seismic events [9,12–15]. Structural conceptual design with respect to static and seismic actions, global layout of the masonry walls, location of the openings, constructive details, material properties, texture of the stone or brickwork, as well as environmental conditions and other parameters were shown to affect the structural response.

Interestingly, the assessment of the quality of the masonry was shown to stand as a prerequisite to any other in-depth study on the existing construction. Quality of the masonry is the result of the quality of the constitutive materials, the effectiveness of the bonding between the elements, the accuracy of the arrangement of the stonework and structural details, level and extension of material decay [3]. The most relevant evidence of poor quality of stoneworks is the absence of mutual-interlocking of the leaves, resulting in three-leaf walls (Figure 1). Conglomerate-like and random rubble stonework, particularly those with rounded pebbles are also acknowledged as poor quality masonry typologies. Other evidences of poor quality are: stacked rather than staggered head joints, irregular and discontinuous bed joints, thick joints, very weak or dusty mortar with no cohesion or no mortar in rubble or pebble stonework, porous stones or bricks with weak bonding to mortar, extended crack patterns, and so forth. [3].

Quality of the masonry plays a major role on both the static and seismic response of the construction. The load bearing capacity under static loads strictly depends on the constructive details of the walls, quality of the materials and their interaction. Poor quality masonry typologies may fail for the onset of local failure mechanisms, such as local detachment and buckling of the masonry leaves, substantially reducing the compressive, shear and flexural strength of the wall [16]. As for the seismic behavior, poor quality of the masonry, particularly in the case of three leaf walls, may dramatically anticipate the failure of the wall, which may be triggered by the out-of-plane overturning of the leeward leaf (Figure 2). In the worst cases, the walls may crumble prior to the onset of the typical local mechanisms under the dynamic excitation induced by the earthquake (Figure 2, [9,14]). The crumbling effect exhibited by poor quality masonry under seismic conditions is emphasized in the case of those superficial earthquakes (typical in the Italian territory) introducing large vertical vibrations, which further weaken the mutual bond between the units, reducing internal compaction of the masonry by extending possible internal micro cracks and spreading local disruption.

Furthermore, quality of the masonry also influences the effectiveness of the most common seismic mitigation measures, such as perimeter ties or floor and roof diaphragms. Perimeter ties rely on the onset of a tied-arch mechanism, with the compressed arch-strut developing within the masonry wall thickness. Poor quality may inhibit the onset of the resisting compressed arch within the masonry wall, and may jeopardize the effectiveness of the tie anchorages by the arch supports [9,17]. Floor and roof diaphragms require effective connections to the masonry walls; whose envisioned performance can only be attained if the connectors are embedded within good quality masonry walls [17,18]. Neither techniques can be therefore addressed until the quality of the masonry has been restored or improved.

Different technical solutions have been proposed to consolidate poor quality masonry walls, such as random rubble stonework or three-leaf stone masonry walls. To date, the upgrade of their static and seismic performances can be pursuit by repointing or deep repointing, grout injections, jacketing and transversal tying of the external leaves, or by partial replacement of masonry wall portions [4,19].

Repointing and deep repointing of the bed-joints consists in the partial replacement of the mortar joints with a new lime-based mortar of improved compactness and durability [20,21]. The mechanical properties of the repointing material should be similar to those of the original wall to avoid abrupt changes in the wall stiffness. In the case of continuous bed joints, the repointing can be strengthened through the insertion of steel or fiber reinforced polymer bars along the bed joints. The effectiveness of this technique may be limited, particularly in the case of very thick walls, provided that the repointing penetration depth is limited. Continuous grid of high strength steel cords placed into the mortar joints, having the nodes secured by means of metal through-rods, may improve the capacity of the wall by also improving the transverse connection of the leaves [22,23].

Injections of low-pressure hydraulic lime-based grouts is a widespread consolidation technique, often suitable for multi-leaf masonries. Injections are aimed at increasing the compactness and consistency of the masonry by filling the internal cracks, voids, collar joints and cavities, thereby improving the bond between the units [24]. Chemical, physical and mechanical compatibility of the grout with the original materials, as well as specific injection protocols are necessary to ensure the efficiency and durability of the intervention. The grout mix-design must be calibrated for each treated wall. Actual injectability of the masonry wall should also be assessed. Injectability depends on the network and percentage of the voids of the inner leaf, which must be sufficiently large as to enable the penetration and diffusion of the grout, but not too large to avoid its percolation and dispersion through the interstices. Also, when the binding of the stone elements is provided by very weak mortar or earthen-based mortars (Figure 1), injections may be ineffective, given that bonding of the injected material to the surface of the stones is unreliable. Particularly in the latter case, the injected grout could hardly adhere to the dirty stone elements, which would not be washed even with extended flushing of clean water. For all these reasons the envisioned strengthening of the masonry wall could not be attained and the effectiveness of the injections must be attentively verified through in-situ testing [25].

Transversal tying of the external leaves significantly improves the interlocking of the leaves and introduces a beneficial confining action, which can be further increased through slight pretension of the ties. The technique inhibits the local buckling of the single leaf, thus increasing the load bearing capacity, and substantially increases the ductility of the masonry walls [3].To be effective, the tie spacing must be sufficiently small, and shorter than the thickness of the wall; only in these conditions the confined masonry core is sufficiently extended to improve the behavior of the masonry wall.

None of these techniques secures the wall with respect to possible disassembly induced by the vertical acceleration typical of superficial earthquakes.

Jacketing with structural plaster and transversal tying of the external leaves is often proposed to improve the in-plane capacity of the stone walls against seismic actions [26]. The existing plaster is removed and the exposed masonry is finished with a new plaster layer. Two different layouts can be adopted: single-side or double-side strengthening. The latter represents the best option as it maintains symmetry along the wall. The technique remarkably increases the in-plane resistance to shear sliding, diagonal tensile cracking, and flexure, depending on the material properties and thickness of the coating layer, as well as on the height-to-thickness ratio of the masonry wall. The beneficial effect is triggered by the additional layers, which can withstand large in-plane actions. Tying rods avoid instability or detachment of the coating layer from the support.

The same technique can also be adopted to increase the load bearing capacity with respect to both vertical and horizontal actions of random rubble and concrete-like stone masonry, whose capacity depends on the internal cohesion, the aggregate interlocking between the elements, and residual tensile strength after cracking, as well as on the possible confinement stress level [16]. In this application, the thin coating, together with the tying steel rods, provides a beneficial restraining confinement action to the masonry cross section, introducing a triaxial stress state, improving ductility and resistance of the existing stonework against both vertical and horizontal actions (Figure 2). To this end, lime based plasters strengthened with GFRP mesh may be adopted [22]. Cement based plaster should be discarded for incompatibility in the case of existing masonry with binding lime mortars. Alternatively, the effectiveness of GFRP mesh inserted into a thin layer made of an inorganic matrix was ascertained by many researchers [27,28]. The technique is quite invasive and does not apply in the presence of valuable plasters or frescoes, nor to listed buildings of historical value or to exposed stonework. However, it is worth noting that in the case of random rabble stone masonry of lower artistic value the technique substantially improves the mechanical properties of the buildings and represents a quite effective retrofit solution. It also provides a vertical tightening restraint against possible masonry disassembly induced by strong vertical acceleration.

By adopting a thermal-insulating plaster, the same technique can be conveniently enhanced to improve the energy efficiency of the construction [22,29], thus generating a tangible benefit that can partly pay for the integrated energy-structural renovation. Due to the poor structural and thermal performances of the existing masonry structures, other combined solutions have recently been proposed for the combined renovation of unreinforced masonry structures. As an example, Triantafillou et al. [30] are studying an innovative structural and energy retrofitting system using TRM combined with thermal insulation. However, although insulating panels are more efficient from an energy point of view than thermal plasters, this system is less adaptable for the application on existing poor quality stone masonry walls.

In this scenario, a new material based on alkali-activated slag is conceived to serve both as structural plaster and as thermo-insulating layer to improve the structural performance and the energy efficiency of poor quality masonry typologies, particularly random rubble stone masonry walls. The use of alkali-activated materials in restoration and conservation of existing structures seems to be very promising due to the outstanding properties at fresh and hardened state [31,32] as well as the durability in severe environments [33–35] and the very low environmental impact [36,37]. However, several topic concerning the compatibility between the substrate and the repair materials [38,39] and the durability in presence of wet and dry cycles [40] need to be better understand. In this paper, the major goals are achieved by adopting a lightweight glass aggregate eco-compatible Portland-free binder based on alkali-activated slag having the compressive strength of a good quality masonry (28-day compressive strength up to 8 MPa) and a reduced specific mass (lower than 1000 kg/m$^3$) in order to reduce the coating layer transmittance. The effectiveness of the reinforcement deriving from the use of alkali-activated slag-based plasters on three leaf masonry wall systems will be the main topic of a future article.

## 2. EXPERIMENTAL PROGRAM

The experimental campaign to characterize the best mortar for the outlined application was planned in two phases. The purpose of the first one was to evaluate the essential characteristics of the mortars at different lightweight aggregate content and to identify the ideal mix proportioning that meets the general requirements in terms of strength and specific mass. In the second stage, several tests were carried out on the previously selected mortar to obtain a more detailed characterization of its behavior, and to evaluate the compatibility between the mortar and the GFRP mesh was investigated by means of mechanical tests and optical microscope observations.

## 2.1 Materials

Three different series of lightweight plasters were manufactured: a traditional Portland-free mortar (hereafter referred as 'TP') manufactured with hydrated lime (HL) CL90-S (according to EN 459-1) and ground granulated blast furnace slag with 28-day pozzolanic activity index equal to 0.76 (GGBFS according to EN 15167-1 and EN 196-5) and two innovative alkali-activated slag-based mixtures (hereafter referred as 'IP') with two different alkaline reagents/precursor ratios. According to Coppola et al. [41], a blend of alkaline reagents in powder form (sodium metasilicate pentahydrate : potassium hydroxide : sodium carbonate = 7 : 3 : 1) was used to produce the innovative plasters with the dosage of the alkaline reagents equal to 20% and 24% by binder mass. The physical properties, the chemical composition and the laser granulometry of binders were reported in Table 1, Table 2 and Figure 3. Moreover, in Figure 4, the XRD pattern of GGBFS was reported, which shows a typical amorphous hump around 25° and 35° 2θ that reflects the short range order of $CaO$-$Al_2O_3$-$MgO$-$SiO_2$ glass structure as reported by Wang and Scrivener [42].

Table 1 – Physical properties of binders (HL: hydrated lime; GGBFS: ground granulated blast furnace slag)

| | $D_{50}$ [μm] | Specific surface [$cm^2/g$] | Specific mass [$g/cm^2$] |
|---|---|---|---|
| HL | 3.00 | 4670 | 2.12 |
| GGBFS | 12.42 | 3440 | 3.13 |

Table 2 - Chemical composition of binders (wt.%) (HL: hydrated lime; GGBFS: ground granulated blast furnace slag)

| | **CaO** | **$Al_2O_3$** | **$SiO_2$** | **$SO_3$** | **$Fe_2O_3$** | **$TiO_2$** | **$K_2O$** | **MgO** |
|---|---|---|---|---|---|---|---|---|
| HL | 94.05 | 1.79 | 1.48 | / | 0.73 | / | / | 1.95 |
| GGBFS | 45.56 | 10.35 | 32.93 | 1.58 | 0.23 | 2.25 | 0.72 | 6.38 |

The water was adjusted in order to attain the same workability at the end of mixing, equal to 160 mm ± 10 mm by means of a flow table. An air-entraining agent (AEA) based on cocamide diethanomaline (according to EN 934-2 and EN 480-2) was added to the mix at 2 kg/m$^3$ to lighten the mortars, reducing, at the same time, the tendency to bleeding and segregation [43]. In addition, the natural siliceous aggregates (NA) were replaced by expanded recycled glass aggregates (EGA), properly combined to meet the Bolomey curve (Table 3 and Figure 5). Alkali activated plasters were prepared using a mixer with planetary motion in accordance with "Dry mixing method" proposed by Bayuaji et al. [44]. In particular, the mixing procedure followed five steps: i) the slag cement, alkaline reagents in powder or flakes, the admixtures and water are placed into the bowl; ii) the mixer starts mixing at low speed for 30 seconds; iii) the aggregates are added to the compound and mixing proceeds at high speed for 60 seconds; iv) the mixing stops for 90 seconds; v) the mixing procedure is completed for further 60 seconds at high speed.

Table 3 – Physical properties of aggregates (NA: Natural siliceous aggregate, EGA: expanded recycled glass aggregates, the numbers represent the particle sizes)

| | Specific mass [g/cm$^3$] | Water absorption [%] |
|---|---|---|
| NA 0 – 0.25 | 2.64 | 0.20 |
| NA 0.25 – 0.50 | 2.70 | 0.76 |
| NA 0.50 – 1.00 | 2.58 | 0.77 |
| NA 1.00 – 2.00 | 2.61 | 0.89 |
| NA 2.00 – 2.50 | 2.62 | 1.02 |
| EGA 0 – 0.50 | 0.70 | 0.86 |
| EGA 0.5 – 1.00 | 0.50 | 0.92 |
| EGA 1.00 – 2.50 | 0.40 | 1.18 |

On the second stage of the experimental campaign, due to the high shrinkage of alkali-activated slag-based materials [45,46], methylcellulose (MC), modified starch (MS), polypropylene fibers (length 6.5 mm, aspect ratio 200, tensile strength 40 MPa, elastic modulus 1.5 GPa) and shrinkage reducing admixture (SRA) were also added to the mortar in order to minimize the risk of cracking and detachments of plaster (Table 4).

Lastly, the properties of the GFRP mesh (epoxy-vinylester resin as a polymer and glass fibers) adopted to reinforce the structural jacketing was reported in Table 5.

Table 4 – Properties of admixtures and fiber (AEA: air-entraining agent, MC: methylcellulose, MS: modified starch, SRA: shrinkage reducing admixture)

| Property | AEA | MC | MS | SRA | Fibers |
|---|---|---|---|---|---|
| Composition | Cocamide diethanolamine | Hydroxypropyl cellulose | Hydroxypropylated starch | Ethylene glycol | Polypropylene |
| Specific mass [$g/cm^3$] | 0.99 | 1.39 | 1.30 | 0.95 | 0.91 |

Table 5 - Properties of the GFRP mesh (provided by the supplier)

| Property | Value | Standard |
|---|---|---|
| Mesh size | 33 x 33 mm | CNR-DT 203/2006 |
| Average thickness | 3 mm | CNR-DT 203/2006 |
| Weight | 1000 $g/m^2$ | -- |
| Glass fiber | Glass AR – $ZrO_2 \geq 16\%$ | ASTM C1666M-07 |
| Polymer | epoxy-vinylester resin | -- |
| Fiber/resin ratio | 65/35 by weight | -- |

## 2.2 First phase

Three different series of plaster (TP, IP20 and IP24) were manufactured by varying the EGA/NA ratio according to the composition reported in Table 6. Workability was measured by means of flow table according to EN 1015-3.  Specific mass at fresh state and entrapped air were detected in accordance with EN 1015-6 and EN 1015-7, respectively. Specimens 40 x 40 x 160 $mm^3$ were produced, cured for 24 hours in mold and then stored in a climatic chamber at 20°C and R.H. 60%. Specific mass at hardened state, compressive and flexural strength were also determined on three specimens for each age and composition (EN 1015-11).

## 2.3 Second phase

During the second stage, several tests were carried out on the mortar that reached the target performances (IP24-100) and on the same mixture manufacturing by adding MC, MS, SRA and fibers

(IP24-100LS) (Tables 7 - 8). In addition to the tests conducted on the first phase, setting time was measured by means of Vicat apparatus (EN 196-3). Secant modulus of elasticity ($E_s$, in accordance with method B, EN 12390-13) on 28-day cured cylindrical specimens (diameter 100 mm, h/d:2) was evaluated by means of compression testing machine (BRT1000) and linear variable displacement transducers applied on the mortar samples. Furthermore, three specimens 40 x 40 x 160 $mm^3$ were used to estimate the 28-day dynamic modulus of elasticity ($E_d$) in accordance with EN 12504-4 (direct transmission). A thin layer of glycerol paste was interposed between the mortar surface and the transducers of the ultrasonic digital indicator tester (UDIT) in order to ensure an adequate acoustical coupling between the specimen and the transducers. The UDIT measures the transmission time of ultrasonic pulse, allowing to calculate the velocity of ultrasonic pulse, note the length of the specimen (160 mm). $E_d$ can be calculated through Equation 1:

$$E_d = \frac{v^2 \rho [(1 - 2\gamma) \cdot (1 + \gamma)]}{(1 - \gamma)} \quad (1)$$

with v: velocity of the ultrasonic pulse (m/s), ρ: specific mass at hardened state ($kg/m^3$) and γ: Poisson's modulus (assumed equal to 0.20) [47]. In addition, bond strength by pull-off was determined on mortars applied with different thicknesses (20 mm and 45 mm) on a traditional brick (5.5 cm x 12 cm x 25 cm) wall after 28 days from casting according to the procedure proposed by EN 1542. Drying shrinkage was also measured over time on prismatic specimens stored 24 hours after the mixing in a climatic chamber at a controlled temperature and humidity (T = 20°C, R.H. = 60%). Moreover, capillary water absorption coefficient of plasters was investigated according to EN 13057. The thermal conductivity of plaster was determined by hot box method using a heat flow meter according to EN 1934 (Figure 6). The mortar was applied on a panel (120 cm x 80 cm) manufactured with lightweight bricks (30 cm x 24.5 cm x 19.5 cm) and traditional Portland cement-based mortar. The thickness of the plaster (applied on both surfaces) was 35 mm. The surface temperatures and the heat flow were measured for 168 hours by setting an internal temperature of 0°C and an external temperature of 20°C. Finally, GFRP mesh was embedded in 400 x 400 x 40 $mm^3$ mortar specimen and GFRP samples were immersed in 1M $Na(OH)_2$ solution in order to evaluate the degradation promoted by the alkaline environment [48] on the epoxy-vinylester resin. The damage degree of GFRP mesh was evaluated through optical microscope observations and measuring the tensile strength loss (ISO 527-4) after 40 days in alkaline environments.

Table 6 - Composition of mortars (nomenclature: TP: traditional lime-based plasters, IP20 and IP24: innovative alkali-activated slag-based plasters with alkaline reagents/binder ratio in mass equal to 20 and 24 respectively, the following number represents the EGA/NA ratio) (GGBFS: ground granulated blast furnace slag; HL: hydrated lime; NA: Natural siliceous aggregate; EGA: expanded recycled glass aggregate; AEA: air-entraining agent)

| | GGBFS [kg/m$^3$] | HL [kg/m$^3$] | Alkaline reagents [kg/m$^3$] | NA [kg/m$^3$] | EGA [kg/m$^3$] | Water [kg/m$^3$] | AEA [kg/m$^3$] |
|---|---|---|---|---|---|---|---|
| TP-0 | 290 | 70 | | 1080 | | 215 | 2 |
| TP-10 | 290 | 70 | | 970 | 25 | 215 | 2 |
| TP-20 | 290 | 70 | | 865 | 55 | 215 | 2 |
| TP-30 | 290 | 70 | | 755 | 80 | 215 | 2 |
| TP-60 | 290 | 70 | | 430 | 160 | 215 | 2 |
| TP-80 | 290 | 70 | | 215 | 210 | 215 | 2 |
| TP-100 | 290 | 70 | | | 265 | 215 | 2 |
| IP20-0 | 275 | | 55 | 990 | | 165 | 2 |
| IP20-10 | 275 | | 55 | 890 | 25 | 165 | 2 |
| IP20-20 | 275 | | 55 | 790 | 50 | 165 | 2 |
| IP20-30 | 275 | | 55 | 690 | 75 | 165 | 2 |
| IP20-60 | 275 | | 55 | 395 | 145 | 165 | 2 |
| IP20-80 | 275 | | 55 | 200 | 195 | 165 | 2 |
| IP20-100 | 275 | | 55 | | 245 | 165 | 2 |
| IP24-0 | 270 | | 65 | 1005 | | 155 | 2 |
| IP24-10 | 270 | | 65 | 905 | 25 | 155 | 2 |
| IP24-20 | 270 | | 65 | 805 | 50 | 155 | 2 |
| IP24-30 | 270 | | 65 | 705 | 75 | 155 | 2 |
| IP24-60 | 270 | | 65 | 400 | 150 | 155 | 2 |
| IP24-80 | 270 | | 65 | 205 | 200 | 155 | 2 |
| IP24-100 | 270 | | 65 | | 250 | 155 | 2 |

Table 7 - Composition of mortars IP24-100 and IP24-100LS (GGBFS: ground granulated blast furnace slag; EGA: expanded recycled glass aggregates with particle sizes; AEA: air-entraining agent; MC: methylcellulose, MS: modified starch, SRA: shrinkage reducing admixture)

| Composition [kg/m$^3$] | IP24-100 | IP24-100LS |
|---|---|---|
| GGBFS | 270 | 270 |
| Alkaline reagents | 65 | 65 |
| EGA | 250 | 250 |
| Water | 155 | 155 |
| AEA | 2 | 2 |
| MC | | 0.40 |
| MS | | 0.15 |
| SRA | | 5.00 |
| Fibers | | 2.70 |

Table 8 - Specimens manufactured for each test

| Test | Ages | Format specimens | Number of specimens |
|---|---|---|---|
| Compressive and flexural strength, specific mass | 1, 7, 28 days | Beam 40x40x160 mm$^3$ | 3 for each ages |
| Secant modulus of elasticity | 28 days | Cylinder h/d : 2<br>d : 100 mm | 6 for each ages |
| Dynamic modulus of elasticity | 28 days | Beam 40x40x160 mm$^3$ | 3 for each ages |
| Bond strength | 28 days | Thickness: 20 and 45 mm | 8 pull-off for each thickness |
| Dry shrinkage | up to 100 days | Beam 40x40x160 mm$^3$ | 3 for each ages |
| Water absorption | 28 days | Beam 40x40x160 mm$^3$ | 3 for each ages |
| Thermal conductivity | 28 days | Thickness: 35 mm | 2 test |

# 3. RESULTS

## 3.1 First phase

### 3.1.1 Rheological properties

The water dosage to obtain the targeted workability varies by varying the type of mortars. In fact, in alkali-activated slag based plasters (IP), the amount of water to achieve 160 mm spreading decreases as the alkaline reagents dosage increases due to the plasticizing and deflocculating effects of sodium silicate explained by Kashani et al. [49]. On the contrary, traditional mortars (TP) require higher mixing water dosages, generally greater than 30-35% compared to the innovative mixtures.

Furthermore, the water content is not affected by the EGA/NA ratio due to the similar water absorption of the aggregates used (Table 6).

The air content of mortars at fresh state does not change as the lightweight aggregate dosage varies (Table 9). On the other hand, the air-entraining agent efficiency seems to be influenced by the nature of binder used (alkali-activated slag or slag/hydrated lime). Indeed, the innovative plasters IP show an entrapped air equal to 35% while the traditional plasters TP are limited to 25%. The specific mass both at fresh and hardened state decrease with the increase of the EGA/NA ratio, independently of binder used (Figure 7-8). In particular, by manufacturing traditional mortars containing only expanded glass aggregates EGA, it is possible to reach density close to 930 kg/m$^3$ at fresh state and 870 kg/m$^3$ at hardened state, while innovative plasters IP exhibit lower densities of about 150 kg/m$^3$ with respect to TP both at fresh and hardened state due to the higher air content.

#### 3.1.2 Mechanical properties

Figure 9-11 show that the mechanical strength of GGBFS/lime-based mortars (TP) are not influenced by the EGA/NA ratio. In fact, regardless of the aggregate used, the compressive strength is quite small (about 2.5 MPa at 28 days). On the contrary, the innovative mortars based on alkali-activated slag (IP) show much higher strength than those measured in traditional plasters, and the compressive strength decreases with the increase of EGA/NA ratio similarly to the specific mass. In detail, the innovative plasters IP manufactured only with expanded glass aggregates guarantee strength between 5.5 MPa (IP20-100) and 8 MPa (IP24-100) with a density at the hardened state close to 700 kg/m$^3$. Furthermore, in Figure 12 it is possible to notice that, for the innovative mixtures, the compressive strength at 28 days from casting is directly proportional to the specific mass. As a matter of fact, the use of an aggregate of poor mechanical properties strongly penalizes the performance of the mortars. On the other hand, according to Neville [43] and Dzturan et al.[50], in presence of a very weak matrix like that of traditional plasters TP, this effect is negligible.

In conclusion, the alkali-activated slag-based plaster manufactured with only expanded glass aggregate IP24-100 combines an extreme lightness (density close to 700 kg/m$^3$) with mechanical strength (28-day compressive strength equal to 8 MPa), which may be considered the upper bound for the use as a thermal reinforced plaster for the upgrade of existing poor quality masonry. Depending on the masonry the strengthening is proposed for, mechanical properties as well as thermal properties can be modified by appropriately modifying the mix design.

Table 9 - Entrapped air and mechanical strength of mortars

| | Entrapped air | Specific mass [kg/m$^3$] | | Compressive strength [MPa] | | |
|---|---|---|---|---|---|---|
| | [%] | Fresh | Hardened | 24 hours | 7 days | 28 days |
| TP-0 | 25 | 1620 | 1540 | 0.51 | 2.41 | 2.57 |
| TP-10 | 25 | 1590 | 1480 | 0.45 | 2.31 | 2.54 |
| TP-20 | 25 | 1470 | 1420 | 0.45 | 2.18 | 2.54 |
| TP-30 | 25 | 1390 | 1380 | 0.44 | 1.99 | 2.40 |
| TP-60 | 25 | 1170 | 1080 | 0.39 | 1.89 | 2.31 |
| TP-80 | 25 | 1050 | 990 | 0.41 | 1.60 | 2.18 |
| TP-100 | 25 | 930 | 870 | 0.40 | 1.39 | 2.03 |
| IP20-0 | 35 | 1510 | 1450 | 6.50 | 11.03 | 13.18 |
| IP20-10 | 35 | 1480 | 1400 | 5.96 | 10.40 | 11.26 |
| IP20-20 | 35 | 1295 | 1230 | 5.68 | 9.88 | 10.34 |
| IP20-30 | 35 | 1250 | 1190 | 4.47 | 7.20 | 8.31 |
| IP20-60 | 35 | 1050 | 990 | 3.94 | 6.72 | 7.89 |
| IP20-80 | 35 | 900 | 830 | 3.12 | 5.46 | 6.18 |
| IP20-100 | 35 | 710 | 690 | 2.85 | 4.89 | 5.51 |
| IP24-0 | 35 | 1550 | 1520 | 7.85 | 12.53 | 15.03 |
| IP24-10 | 35 | 1500 | 1460 | 6.75 | 11.52 | 13.28 |
| IP24-20 | 35 | 1360 | 1330 | 6.87 | 11.02 | 11.95 |
| IP24-30 | 35 | 1290 | 1250 | 6.29 | 10.36 | 10.88 |
| IP24-60 | 35 | 1100 | 1070 | 5.67 | 9.89 | 10.23 |
| IP24-80 | 35 | 970 | 920 | 3.49 | 9.03 | 9.86 |
| IP24-100 | 35 | 760 | 720 | 2.85 | 7.17 | 8.26 |
| IP24-100 LS | 35 | 770 | 725 | 2.91 | 7.24 | 8.19 |

## 3.2 Second phase

In this stage, the results of the tests carried out on the mortar that reached the target performances will be presented. In particular, the properties of mortars manufactured with (IP24-100LS) and without (IP24-100) the addition of MC, MS, SRA and fibers were analyzed. Finally, the results of the test carried out on the GFRP mesh will be presented.

### 3.2.1 Rheological properties

The addition of admixtures able to reduce the shrinkage-induced cracking does not change the amount of water at equal workability, specific mass and air content. Furthermore, the initial and final set measured by needle of Vicat (50 minutes initial set, 140 minutes final set) are similar to those of traditional plasters based on Portland cement and lime [51], resulting perfectly compatible with the construction needs.

### 3.2.2 Elasto-mechanical properties

There are no changes in the mechanical strength between the mortar IP24-100 and IP24-100LS (Table 9). The addition of ethylene glycol, unlike on traditional Portland mixture [52] or on normal-weight alkali-activated slag-based mortars [53,54], does not appear to affect negatively the development of elasto-mechanical properties of alkali-activated slag-based plaster manufactured with only expanded glass aggregate. The elastic modulus of IP mortars is very low, close to 1.5 GPa for the secant modulus $E_s$ and 2.50 GPa for the dynamic modulus $E_d$ (Table 10). The Young's modulus of the IP is so low because this property depends strongly on the rigidity of the aggregate and on the characteristics of the binder paste [43]. The EGA have poor elasto-mechanical properties that thus minimize the stiffness of the mortar. Moreover, at the same strength class, Coppola et al. [55] and Thomas et al. [56] have shown that alkali-activated slag-based mortars are characterized by lower elastic modulus than those Portland cement mortars. The reduction of $E_d$ and $E_s$ in IP respect to TP is a consequence of the high shrinkage of slag-based mortars which caused microcrack formation.

Table 10 - Elastic modulus of mortars

| | IP24-100 | IP24-100LS |
|---|---|---|
| $E_s$ [GPa] | 1.50 | 1.50 |
| ρ [kg/m$^3$] | 870 | 875 |
| v [km/s] | 1.85 | 1.85 |
| $E_d$ [GPa] | 2.50 | 2.50 |

### 3.2.3 Shrinkage

Dry shrinkage of innovative plaster is given in Figure 13 that shows very high free shrinkage of alkali-activated materials compared to mixtures manufactured with traditional binders, as widely reported in the scientific literature [45,57,58]. The addition of admixtures and fiber reduced shrinkage in alkali-activated slag mortars by up to 50%. Palacios et al. [53] explains that this beneficial effect of the shrinkage reducing admixture (SRA) is primarily due to: firstly, the decrease in the surface tension of water in the porous system and the concomitantly smaller internal stress when the water evaporates; secondly, and most importantly, the redistribution of the porous structure, because the admixture increases the percentage of pores with diameters ranging from 0.1 to 1.0 µm, which exhibit a capillary stress much lower than the smaller pores that prevail in mortars without admixture. This redistribution of the pores is due to the decrease of the capillary stress of the water that SRA induces during the mixing process.

Furthermore, due to the low elastic modulus and the limited shrinkage of innovative plaster, tensile stress induced by restrained shrinkage is still low, preventing the mortars from cracks and detachments. This behavior was verified through the application of thin layers of plaster on brick stored in extra-dry conditions (R.H. < 30%) to emphasize the risk of cracking and detachment (Figure 14). In particular, a 2 cm-thick layer of IP24-100 after a few days was totally detached from the support, while the plaster manufactured with the addition of admixtures and fibers IP24-100LS showed no detachments or cracking up to 1 year. Moreover, no cracks were observed on the panels used for thermal conductivity (Figure 6) and adhesion tests.

### 3.2.4 Bond strength

The bond strength between alkali-activated slag-based plasters and the masonry is one of the key engineering properties for this kind of applications. In particular, it requires the jacketing to be strongly adhesive to the substrate after final setting. As it can be seen from Table 11, the bond strength values are higher when the mortar has been applied with a lower thickness. In the case with s= 45 mm a 100% cohesion failure was observed in the alkali activated mortar layer, indicating that the repair material is the weakest part of the system. This behavior is probable due to the greater probability of finding faults that strongly influence the tensile strength of the material. On the other hand, the failure type was more variable in the case with s=20 mm, where the observed failures were both cohesion failure in the mortar layer and adhesion failure along the interface surface (Figure 15).

Table 11 - Bond strength of mortars IP24-100LS applied on the substrate with two different thicknesses (t=20mm and 45mm)

| | Adhesion strength [MPa] and failure type | | | |
|---|---|---|---|---|
| | t = 20 mm | | t = 45 mm | |
| 1 | 1.05 | Cohesive | 0.17 | Cohesive |
| 2 | 0.68 | Cohesive | 0.23 | Cohesive |
| 3 | 0.59 | Cohesive | 0.50 | Cohesive |
| 4 | 0.93 | Interface | 0.31 | Cohesive |
| 5 | 1.16 | Cohesive | 0.41 | Cohesive |
| 6 | 1.01 | Interface | 0.44 | Cohesive |
| 7 | 1.04 | Interface | 0.20 | Cohesive |
| 8 | 0.64 | Interface | 0.38 | Cohesive |

### 3.2.5 Thermal properties and energy saving

The conductivity of ordinary concrete strongly depends on its composition. In general, density does not appreciably affect the conductivity of ordinary concrete, however, due to the low conductivity of air, the thermal conductivity of lightweight concrete varies with its density. The method to determine the thermal resistance of plaster requires the measurement of surface temperatures and heat-flux through the test wall by the use of heat-flux meters. The thermal resistance R is given by:

$$R_{tot} = \frac{\sum_{j=1}^{n} T_{swj} - T_{scj}}{\sum_{j=1}^{n} q_j} \text{ con j = 1 ,…., n} \tag{2}$$

with: $T_{sw}$ = surface temperature on the test wall warm side [K]

$T_{sc}$ = surface temperature on the test wall cold side [K]

q = transmission heat loss through a wall per unit area [W/m$^2$].

Note the thermal resistance of the brick wall $R_{bw}$, the thermal resistance of the plaster $R_p$ can be obtained according to the following relationship:

$$R_p = R_{tot} - R_{bw} \quad (3)$$

The thermal conductivity λ of the plaster is obtained from the ratio between the thickness (t) of the plaster layer during the test and the thermal resistance of the product.

Table 12 - Thermal properties of plasters

| | IP24-100LS | LP |
|---|---|---|
| Thermal resistance $R_p$ [$m^2K/W$] | 0.101 | -- |
| Thickness $t_p$ [mm] | 35 | -- |
| Thermal conductivity $\lambda_p$ [W/mK] | 0.35 | 0.80 |

The value of the thermal conductivity of the lightweight plaster (0.35 W/mK) is lower by about 75% compared to a traditional mortar based on Portland cement and lime (~ 1.30 W/mK) [43]. On the other hand, comparing the thermal conductivity of IP24-100LS with those of a traditional lime plaster (LP), the difference between the conductivity values is around 55% at equal strength class (Table 12) [59]. This behavior is due to the replacement of traditional aggregates with expanded recycled glass aggregates [43].

Furthermore, by using a building thermal modeling computer program [60], the energy consumption of a 100 $m^2$-detached house in central Apennine mountains (L'Aquila, Italy) was evaluated by varying the thermal properties of reinforced plaster used. In particular, the simulation was carried out with two reinforced plasters (IP24-100LS and LP) applied with a thickness of 6 cm on a stone masonry wall. As reported in Table 13, the use of lightweight mortar instead of traditional reinforced plaster on a stone masonry building leads to a reduction in energy consumption up to 31 $kWh/m^2$ year (-20%).

Table 13 - Thermal properties of detached house estimated adopting a building thermal modeling computer program [49]

| | IP | IP-LP | LP |
|---|---|---|---|
| Stratigraphy | IP-masonry-IP | IP-masonry-LP | LP-masonry-LP |
| Thickness [cm] | 6 + 60 + 6 | 6 + 60 + 6 | 6 + 60 + 6 |
| Wall thermal transmittance [W/m$^2$K] | 1.277 | 1.458 | 1.712 |
| Building energy consumption [kWh/m$^2$ year] | 165 | 146 | 134 |
| Energy saving [%] | - 20% | -12% | -- |

### 3.2.6 Water absorption

The absorption coefficient of the lightweight plaster (2.78 kg/m$^2$h$^{0.5}$) is higher compared to a traditional mortar based on Portland cement and lime (~1.63 kg/m$^2$h$^{0.5}$) [43]. A higher value of absorption coefficient could cause a reduction in thermal resistance of plaster on site, due to the water saturation of external layer during raining periods. For this reason, an alchil-alcoxisilane-based coating was applied on IP24-100LS surface in order to reduce the water absorption of mortar. As reported in Figure 16, applying the waterproofing material, is possible to reduce the absorption coefficient up to 80%, reducing the risk of saturation of the plaster and, hence, preserving the thermal resistance of the external plaster.

### 3.2.7 Characterization of the GFRP mesh

The potential degradation promoted by the alkaline environment on the GFRP mesh is finally evaluated. The GFRP mesh consists of two types of fiber (twist and flat). The tensile ultimate load of fibers was evaluated (ISO 527-4) and values similar to those shown in the technical data sheet were obtained. In particular, the fiber failure occurred for tensile loads close to 2.05 kN for twist fibers and 3.37 kN for flat fibers.

The same tests were carried out after 40 days of embedding in the lightweight plaster IP24-100LS or after 7 days in $Na(OH)_2$ solution. However, strength losses were not observed following exposure to strongly alkaline environments (Tab. 14). In addition to the tensile test, optical microscope observations were also carried out. Figure 17 shows the GFRP mesh exposed to different environments: reference fibers (left), fibers after 40 days embedded in lightweight plaster (center), fibers after 7 days in 1M $Na(OH)_2$ solution (right). It is possible to observe that the GFRP mesh, especially the resin surface, did not suffer any degradation.

*Table 14 – Tensile load of GFRP in different environment*

| | Tensile load [kN] | | |
|---|---|---|---|
| | As received | After 40 days in plaster | After 7 days in 1M $Na(OH)_2$ solution |
| Twist fibers | 2.05 | 1.99 | 2.01 |
| Flat fibers | 3.37 | 3.20 | 3.27 |

## 4. CONCLUSION

In this paper, a lightweight cement-free reinforced plaster to be applied in GFRP-reinforced jacketing interventions for the energy upgrading and seismic retrofitting of poor quality masonry buildings was developed. Analyzing the experimental data, it is possible to conclude that:

- The use of expanded recycled glass aggregates (EGA) instead of natural siliceous aggregates (NA) and the addition of air-entraining agent (AEA) reduce the specific mass at fresh and hardened state of mortars up to 750 kg/m$^3$;
- The traditional plaster TP provides mechanical strength of about 2-2.5 MPa, while the Portland-free plaster IP24-100LS is able to provide a 28-day compressive strength equal to 8 MPa and a thermal conductivity of 0.35 W/mK due to density close to 700 kg/m$^3$, which match the target fixed in this research as the upper bound for this kind of applications;
- The high free-shrinkage of alkali-activated slag based-plaster was strongly reduced by using a blend of admixtures that are able to reduce the shrinkage to values close to those of Portland-based mortars;
- The reduced shrinkage and the low elastic modulus ensure an excellent adhesion to the substrate (up to 1.16 MPa) and the absence of micro-cracks and detachments;

- By using an alchil-alcoxisilane-based coating is possible to reduce the water absorption of mortar up to 80%, avoiding the saturation of plaster on site during raining periods;
- The GFRP mesh showed a high resistance to alkaline environments and is therefore perfectly suitable for this type of application.


## ACKNOWLEDGEMENTS

The authors would like to acknowledge prof. Alberto Arenghi and the PISA Laboratory of the University of Brescia for the support in the experimental tests to determine the thermal properties of the mortar and Eng. Ilaria Baroni and Andrea Mazzoleni for the development of the tests during their Master Thesis. This research did not receive any specific grant from founding agencies in the public, commercial or not-for-profit sectors.

## LIST OF FIGURES

## REFERENCES


[1] M. Shuller, R. Atkinson, J. Noland, Structural evaluation of historic masonry buildings, APT Bull. J. Preserv. Technol. 26 (1995) 51–61.

[2] L. Binda, A. Saisi, C. Tiraboschi, Investigation procedures for the diagnosis of historic masonries, Constr. Build. Mater. 14 (2000) 199–233. doi:10.1016/S0950-0618(00)00018-0.

[3] A. Borri, M. Corradi, G. Castori, A. De Maria, A method for the analysis and classification of historic masonry, Bull. Earthq. Eng. 13 (2015) 2647–2665. doi:10.1007/s10518-015-9731-4.

[4] M.R. Valluzzi, F. Da Porto, C. Modena, Behavior and modeling of strengthened three-leaf stone masonry walls, Mater. Struct. Constr. 37 (2004) 184–192. doi:10.1617/13977.

[5] P.B. Lourenço, N. Mendes, L.F. Ramos, D. V. Oliveira, Analysis of masonry structures without box behavior, Int. J. Archit. Herit. 5 (2011) 369–382. doi:10.1080/15583058.2010.528824.

[6] M. Rota, A. Penna, G. Magenes, A framework for the seismic assessment of existing masonry buildings accounting for different sources of uncertainty, Earthq. Eng. Struct. Dyn. 43 (2014) 1045–1066. doi:10.1002/eqe.2386.

[7] B. Silva, A.E. Pigouni, M.R. Valluzzi, C. Modena, Calibration of analytical formulations predicting compressive strength in consolidated three-leaf masonry walls, Constr. Build. Mater. 64 (2014) 28–38. doi:10.1016/j.conbuildmat.2014.04.044.

[8] A. Avorio, A. Borri, G. Cangi, Riparazione e consolidamento degli edifici in muratura, in: Man. per La Riabil. e La Ricostr. Post Sismica Degli Edif., DEI editio, Rome, 1999.

[9] E. Giuriani, A. Marini, Experiences from the Northern Italy 2004 earthquake: vulnerability

assessment and strengthening of historic churches, in: Proc. VI Int. Conf. Struct. Anal. Hist. Constr. SAHC - Bath, 2008: pp. 13–24.

[10] E.P. Giuriani, A. Marini, M. Preti, Thin-folded Shell for the Renewal of Existing Wooden Roofs, Int. J. Archit. Herit. 10 (2016) 797–816. doi:10.1080/15583058.2015.1075626.

[11] L. Ferrario, A. Marini, P. Riva, E. Giuriani, Traditional and innovative techniques for the seismic strengthening of barrel vaulted structures subjected to rocking of the abutments, in: Proc. ATC-SEI Conf. Improv. Seism. Perform. Exist. Build. Other Struct. - San Fr., American Society of Civil Engineers, Reston, VA, 2009. doi:10.1061/41084(364)122.

[12] S. Lagomarsino, S. Podestà, Seismic vulnerability of ancient churches: II. Statistical analysis of surveyed data and methods for risk analysis, Earthq. Spectra. 20 (2004) 395–412. doi:10.1193/1.1737736.

[13] E. Giuriani, A. Marini, C. Porteri, M. Preti, Seismic vulnerability for churches in association with transverse arch rocking, Int. J. Archit. Herit. 3 (2009) 212–234. doi:10.1080/15583050802400240.

[14] D.F. D'Ayala, S. Paganoni, Assessment and analysis of damage in L'Aquila historic city centre after 6th April 2009, Bull. Earthq. Eng. 9 (2011) 81–104. doi:10.1007/s10518-010-9224-4.

[15] I. Senaldi, G. Magenes, J. Ingham, Performance of unreinforced stone masonry buildings during the 2010/2011 Canterbury earthquake swarm and retrofit techniques for their seismic improvement, SESOC J. 24 (2011) 44.

[16] S. Cominelli, E. Giuriani, A. Marini, Mechanisms governing the compressive strength of unconfined and confined rubble stone masonry, Mater. Struct. Constr. 50 (2017) 10. doi:10.1617/s11527-016-0905-6.

[17] A. Marini, E. Giuriani, A. Belleri, S. Cominelli, Dowel connections securing roof-diaphragms to perimeter walls in historic masonry buildings and in-field testing for capacity assessment, Bull. Earthq. Eng. 16 (2018) 4001–4025. doi:10.1007/s10518-018-0333-9.

[18] E. Giuriani, A. Marini, Wooden roof box structure for the anti-seismic strengthening of historic buildings, Int. J. Archit. Herit. 2 (2008) 226–246. doi:10.1080/15583050802063733.

[19] L. Binda, C. Modena, G. Baronio, S. Abbaneo, Repair and investigation techniques for stone masonry walls, Constr. Build. Mater. 11 (1997) 133–142. doi:10.1016/S0950-0618(97)00031-7.

[20] M.R. Valluzzi, L. Binda, C. Modena, Mechanical behaviour of historic masonry structures strengthened by bed joints structural repointing, Constr. Build. Mater. 19 (2005) 63–73. doi:10.1016/j.conbuildmat.2004.04.036.

[21] E. Garbin, M.R. Valluzzi, C. Modena, Testing and numerical modelling of the structural behaviour of brick masonry strengthened by the bed joints reinforcement technique, in: Proc. 1st WTA Int. PhD Symp. - Build. Mater. Build. Technol. to Preserv. Built Herit. - Leuven, 2009: pp. 489–516.

[22] A. Borri, M. Corradi, R. Sisti, C. Buratti, E. Belloni, E. Moretti, Masonry wall panels retrofitted with thermal-insulating GFRP-reinforced jacketing, Mater. Struct. Constr. 49 (2016) 3957–3968. doi:10.1617/s11527-015-0766-4.

[23] M. Corradi, A. Borri, G. Castori, R. Sisti, The Reticulatus method for shear strengthening of fair-faced masonry, Bull. Earthq. Eng. 14 (2016) 3547–3571. doi:10.1007/s10518-016-0006-5.

[24] D. V. Oliveira, R.A. Silva, E. Garbin, P.B. Lourenĉo, Strengthening of three-leaf stone masonry walls: An experimental research, Mater. Struct. Constr. 45 (2012) 1259–1276.

doi:10.1617/s11527-012-9832-3.

[25] M.R. Valluzzi, E. Cescatti, G. Cardani, L. Cantini, L. Zanzi, C. Colla, F. Casarin, Calibration of sonic pulse velocity tests for detection of variable conditions in masonry walls, Constr. Build. Mater. 192 (2018) 272–286. doi:https://doi.org/10.1016/j.conbuildmat.2018.10.073.

[26] M. Corradi, A. Borri, G. Castori, R. Sisti, Shear strengthening of wall panels through jacketing with cement mortar reinforced by GFRP grids, Compos. Part B Eng. 64 (2014) 33–42. doi:10.1016/j.compositesb.2014.03.022.

[27] N. Gattesco, A. Dudine, Effectiveness of masonry strengthening technique made with plaster reinforced with a GFRP net, in: Proc. 8th Int. Mason. Conf. - Dresden, 2010.

[28] F. Parisi, I. Iovinella, A. Balsamo, N. Augenti, A. Prota, In-plane behaviour of tuff masonry strengthened with inorganic matrix-grid composites, Compos. Part B Eng. 45 (2013) 1657–1666. doi:10.1016/j.compositesb.2012.09.068.

[29] L. Coppola, D. Coffetti, S. Lorenzi, Cement-Based Renders Manufactured with Phase-Change Materials: Applications and Feasibility, Adv. Mater. Sci. Eng. 2016 (2016). doi:10.1155/2016/7254823.

[30] T.C. Triantafillou, K. Karlos, K. Kefalou, E. Argyropoulou, An innovative structural and energy retrofitting system for URM walls using textile reinforced mortars combined with thermal insulation: Mechanical and fire behavior, Constr. Build. Mater. 133 (2017) 1–13. doi:10.1016/J.CONBUILDMAT.2016.12.032.

[31] J.G. Jang, N.K. Lee, H.K. Lee, Fresh and hardened properties of alkali-activated fly ash/slag pastes with superplasticizers, Constr. Build. Mater. 50 (2014) 169–176. doi:10.1016/J.CONBUILDMAT.2013.09.048.

[32] S. Bernal, R. San Nicolas, J. Provis, J.S.J. van Deventer, Alkali-activated slag cements produced with a blended sodium carbonate / sodium silicate activator, Adv. Cem. Res. (2015) 1–12. doi:dx.doi.org/10.1680/adcr.15.00013.

[33] A. Leemann, H. Pahlke, R. Loser, F. Winnefeld, Carbonation resistance of mortar produced with alternative cements, Mater. Struct. Constr. 51 (2018) 114. doi:10.1617/s11527-018-1239-3.

[34] F. Shahrajabian, K. Behfarnia, The effects of nano particles on freeze and thaw resistance of alkali-activated slag concrete, Constr. Build. Mater. 176 (2018) 172–178. doi:10.1016/j.conbuildmat.2018.05.033.

[35] T. Bakharev, J.G. Sanjayan, Y.B. Cheng, Sulfate attack on alkali-activated slag concrete, Cem. Concr. Res. 32 (2002) 211–216. doi:10.1016/S0008-8846(01)00659-7.

[36] L. Coppola, Binders alternative to Portland cement and waste management for sustainable construction—part 1, J. Appl. Biomater. Funct. Mater. 16 (2018) 186–202. doi:10.1177/2280800018782845.

[37] L. Coppola, D. Coffetti, E. Crotti, G. Gazzaniga, T. Pastore, An Empathetic Added Sustainability Index (EASI) for cementitious based construction materials, J. Clean. Prod. 220 (2019) 475–482. doi:10.1016/j.jclepro.2019.02.160.

[38] S. Kramar, A. Šajna, V. Ducman, Assessment of alkali activated mortars based on different precursors with regard to their suitability for concrete repair, Constr. Build. Mater. 124 (2016) 937–944. doi:10.1016/j.conbuildmat.2016.08.018.

[39] R.H. Geraldo, O.G. Teixeira, S.R.C. Matos, F.G.S. Silva, J.P. Gonçalves, G. Camarini, Study of alkali-activated mortar used as conventional repair in reinforced concrete, Constr. Build. Mater. 165 (2018) 914–919. doi:10.1016/j.conbuildmat.2018.01.063.

[40] A. Allahverdi, E. Najafi Kani, B. Shaverdi, Carbonation Versus Efflorescence in Alkali-Activated Blast-Furnace Slag in Relation with Chemical Composition of Activator, Int. J. Civ. Eng. 15 (2017) 565–573. doi:10.1007/s40999-017-0225-4.

[41] L. Coppola, D. Coffetti, E. Crotti, Pre-packed alkali activated cement-free mortars for repair of existing masonry buildings and concrete structures, Constr. Build. Mater. 173 (2018) 111–117. doi:10.1016/j.conbuildmat.2018.04.034.

[42] S.-D. Wang, K.L. Scrivener, Hydration products of alkali activated slag cement, Cem. Concr. Res. 25 (1995) 561–571.

[43] A.M. Neville, Properties of concrete, Longman London, 1995.

[44] R. Bayuaji, A.K. Yasin, T.E. Susanto, M.S. Darmawan, S. Darmawan, A review in geopolymer binder with dry mixing method (geopolymer cement), AIP Conf. Proc. 1887 (2017) 20042. doi:10.1063/1.5003513.

[45] H. Ye, A. Radlińska, Shrinkage mechanisms of alkali-activated slag, Cem. Concr. Res. 88 (2016) 126–135.

[46] C. Cartwright, F. Rajabipour, A. Radlińska, Shrinkage Characteristics of Alkali-Activated Slag Cements, J. Mater. Civ. Eng. 27 (2015) B4014007. doi:10.1061/(ASCE)MT.1943-5533.0001058.

[47] R. Narayan Swamy, Dynamic Poisson's ratio of portland cement paste, mortar and concrete, Cem. Concr. Res. 1 (1971) 559–583. doi:10.1016/0008-8846(71)90060-3.

[48] T. Bakharev, J.G. Sanjayan, Y.B. Cheng, Resistance of alkali-activated slag concrete to acid attack, Cem. Concr. Res. 33 (2003) 1607–1611. doi:10.1016/S0008-8846(03)00125-X.

[49] A. Kashani, J.L. Provis, G.G. Qiao, J.S.J. Van Deventer, The interrelationship between

surface chemistry and rheology in alkali activated slag paste, Constr. Build. Mater. 65 (2014) 583–591. doi:10.1016/j.conbuildmat.2014.04.127.

[50] T. Dzturan, C. Ceqen, Effect of coarse aggregate type on mechanical properties of concretes with different strengths, Cem. Concr. Res. 27 (1997) 165–170.

[51] B.A. Silva, A.P. Ferreira Pinto, A. Gomes, Natural hydraulic lime versus cement for blended lime mortars for restoration works, Constr. Build. Mater. 94 (2015) 346–360. doi:10.1016/j.conbuildmat.2015.06.058.

[52] V. Corinaldesi, Combined effect of expansive, shrinkage reducing and hydrophobic admixtures for durable self compacting concrete, Constr. Build. Mater. 36 (2012) 758–764. doi:10.1016/j.conbuildmat.2012.04.129.

[53] M. Palacios, F. Puertas, Effect of shrinkage-reducing admixtures on the properties of alkali-activated slag mortars and pastes, Cem. Concr. Res. 37 (2007) 691–702. doi:10.1016/j.cemconres.2006.11.021.

[54] V. Bílek, L. Kalina, R. Novotný, J. Tkacz, L. Pařízek, Some Issues of Shrinkage-Reducing Admixtures Application in Alkali-Activated Slag Systems, Materials (Basel). 9 (2016) 462. doi:10.3390/ma9060462.

[55] L. Coppola, D. Coffetti, E. Crotti, One-Part Alkali-Activated Slag Cement for Conservation of Existing Structures, ACI Spec. Publ. 330 (2018) 107–122.

[56] R.J. Thomas, S. Peethamparan, Alkali-activated concrete: Engineering properties and stress–strain behavior, Constr. Build. Mater. 93 (2015) 49–56.

[57] H. Ye, A. Radlińska, Shrinkage mitigation strategies in alkali-activated slag, Cem. Concr. Res. 101 (2017) 131–143. doi:10.1016/j.cemconres.2017.08.025.

[58] X.H. Yuan, W. Chen, Z.A. Lu, H. Chen, Shrinkage compensation of alkali-activated slag concrete and microstructural analysis, Constr. Build. Mater. 66 (2014) 422–428. doi:10.1016/j.conbuildmat.2014.05.085.

[59] R. Walker, S. Pavia, Thermal and hygric properties of insulation materials suitable for historic fabrics, in: Proc. III Int. Congr. Constr. Build. Res., 2015.

[60] D.B. Crawley, L.K. Lawrie, C.O. Pedersen, F.C. Winkelmann, Energy plus: energy simulation program, ASHRAE J. 42 (2000) 49–56.

a)

b)


a)


b)

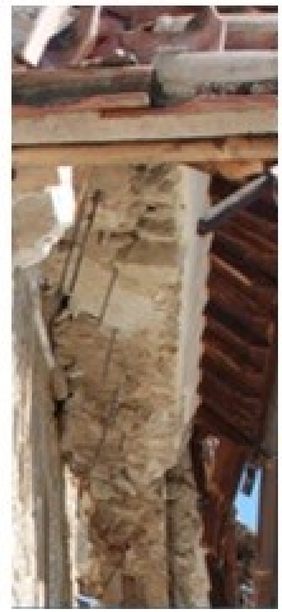
c)

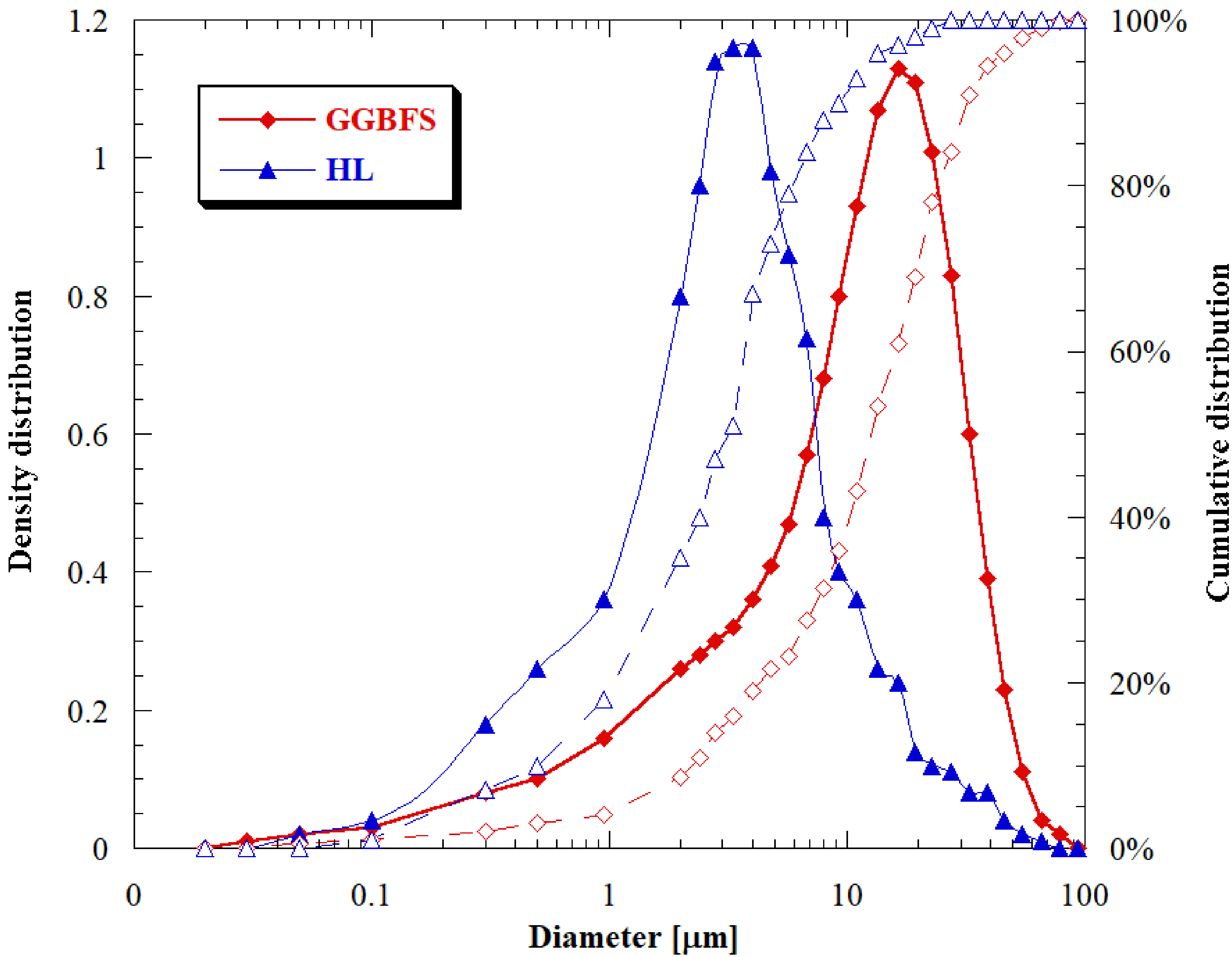
GGBFS
HL
Density distribution
Cumulative distribution
Diameter [μm]
0
0.1
1
10
100
0.2
0.4
0.6
0.8
1.2
0%
20%
40%
60%
80%
100%

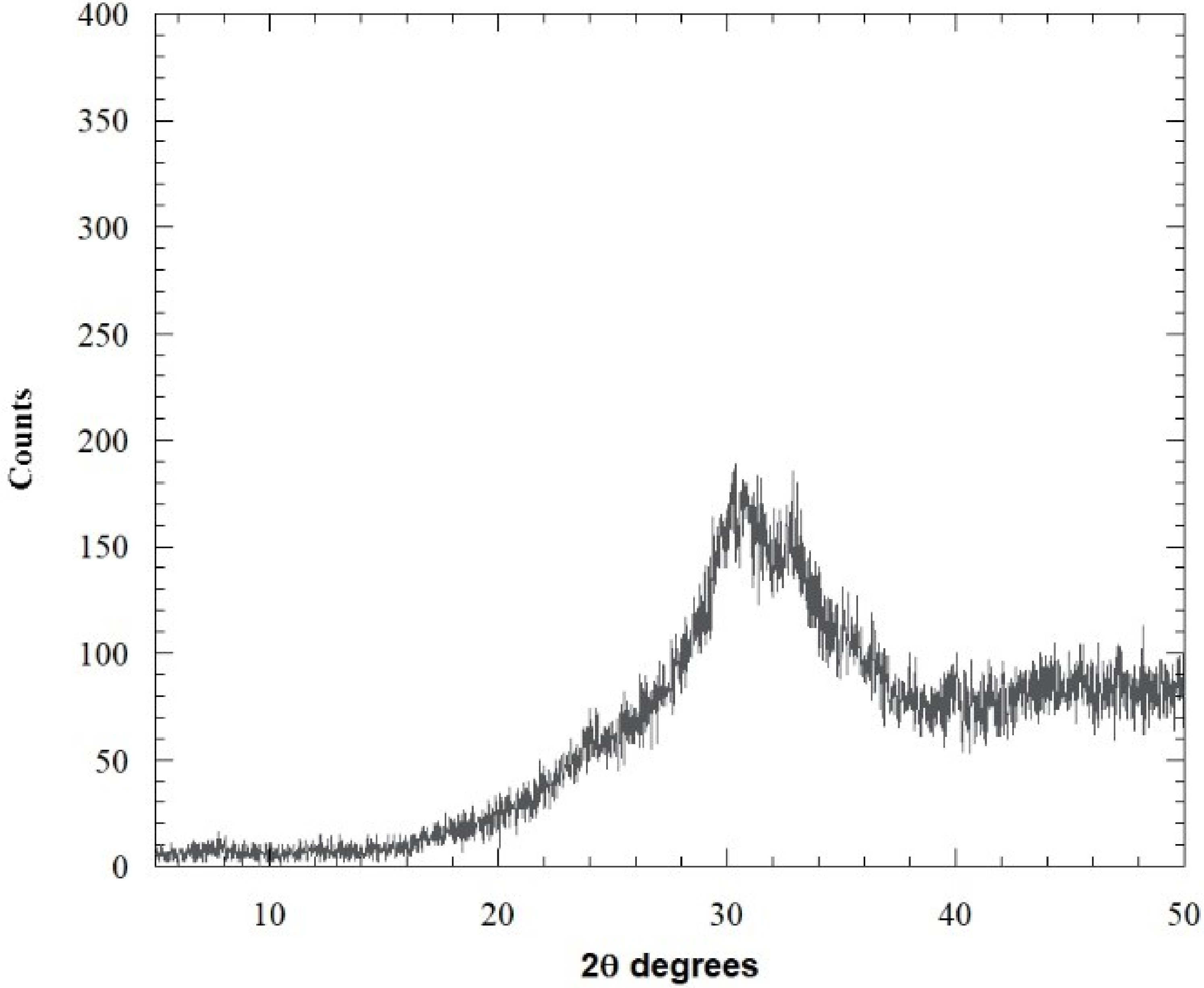
400
350
300
250
200
150
100
50
0
Counts
10
20
30
40
50
2θ degrees

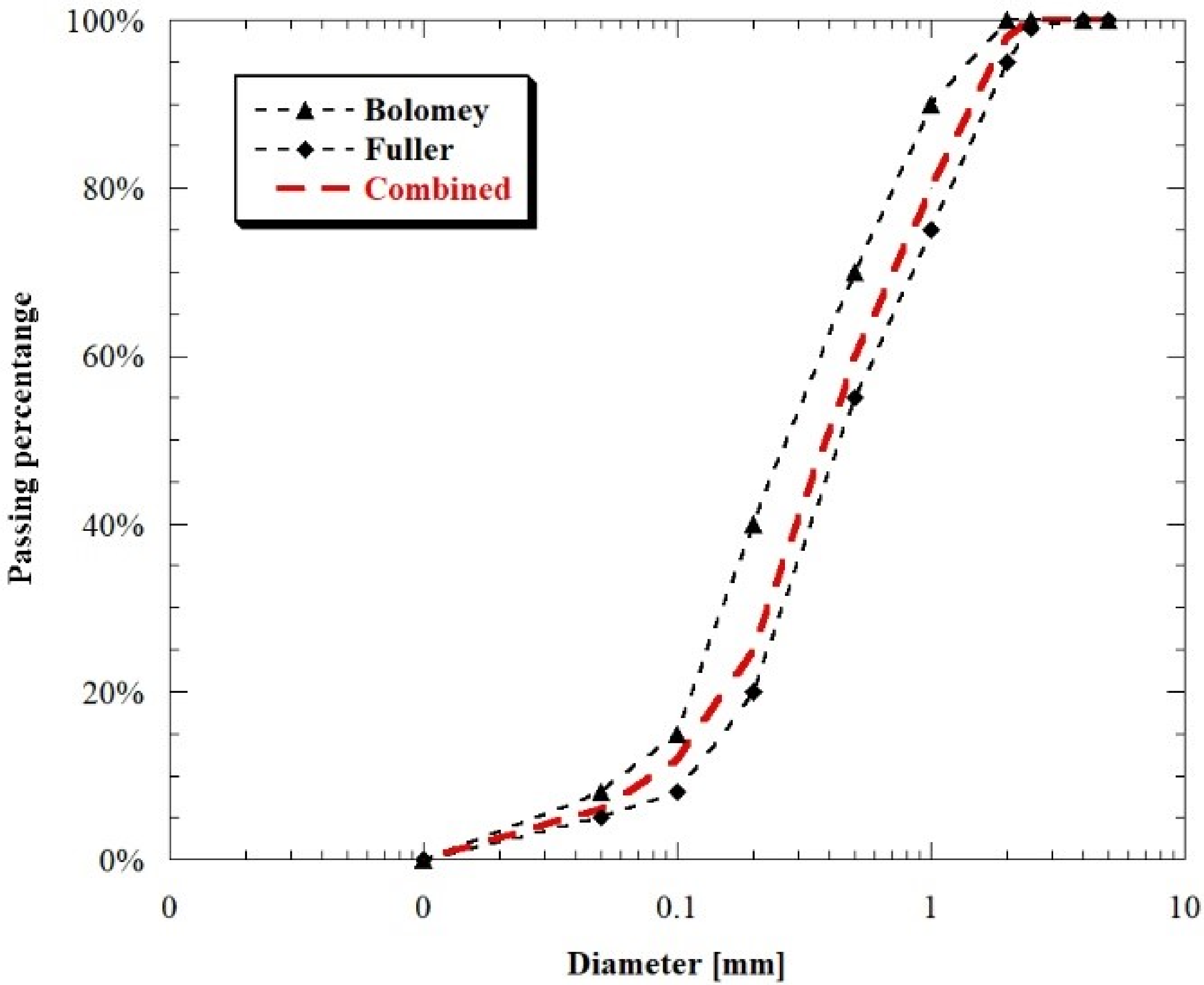

Bolomey
Fuller
Combined
100%
80%
60%
40%
20%
0%
Passing percentange
0
0
0.1
1
10
Diameter [mm]



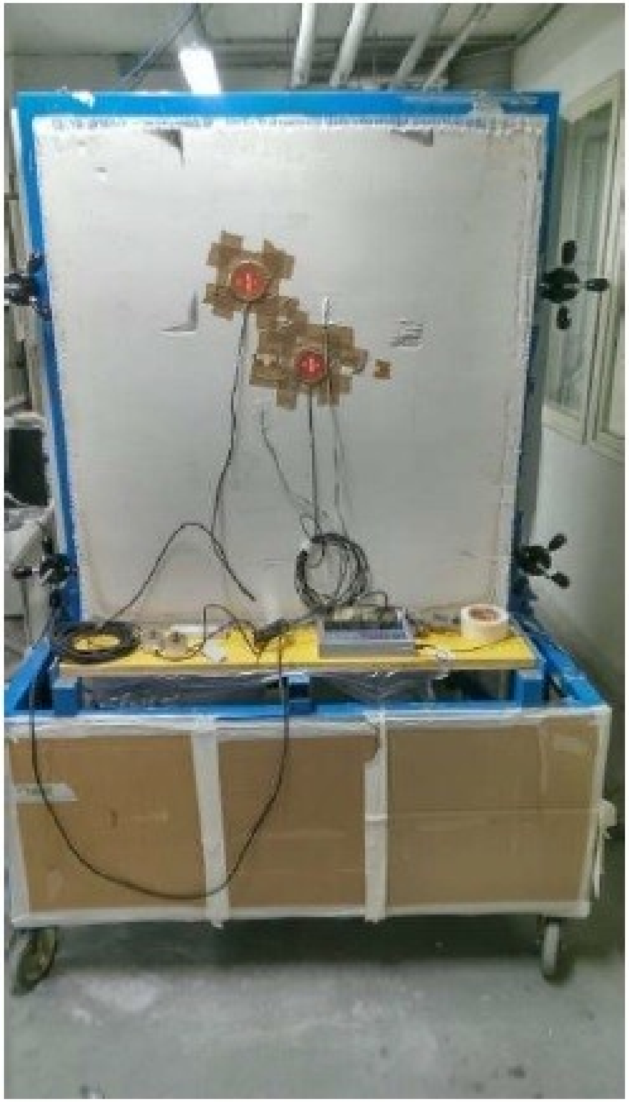

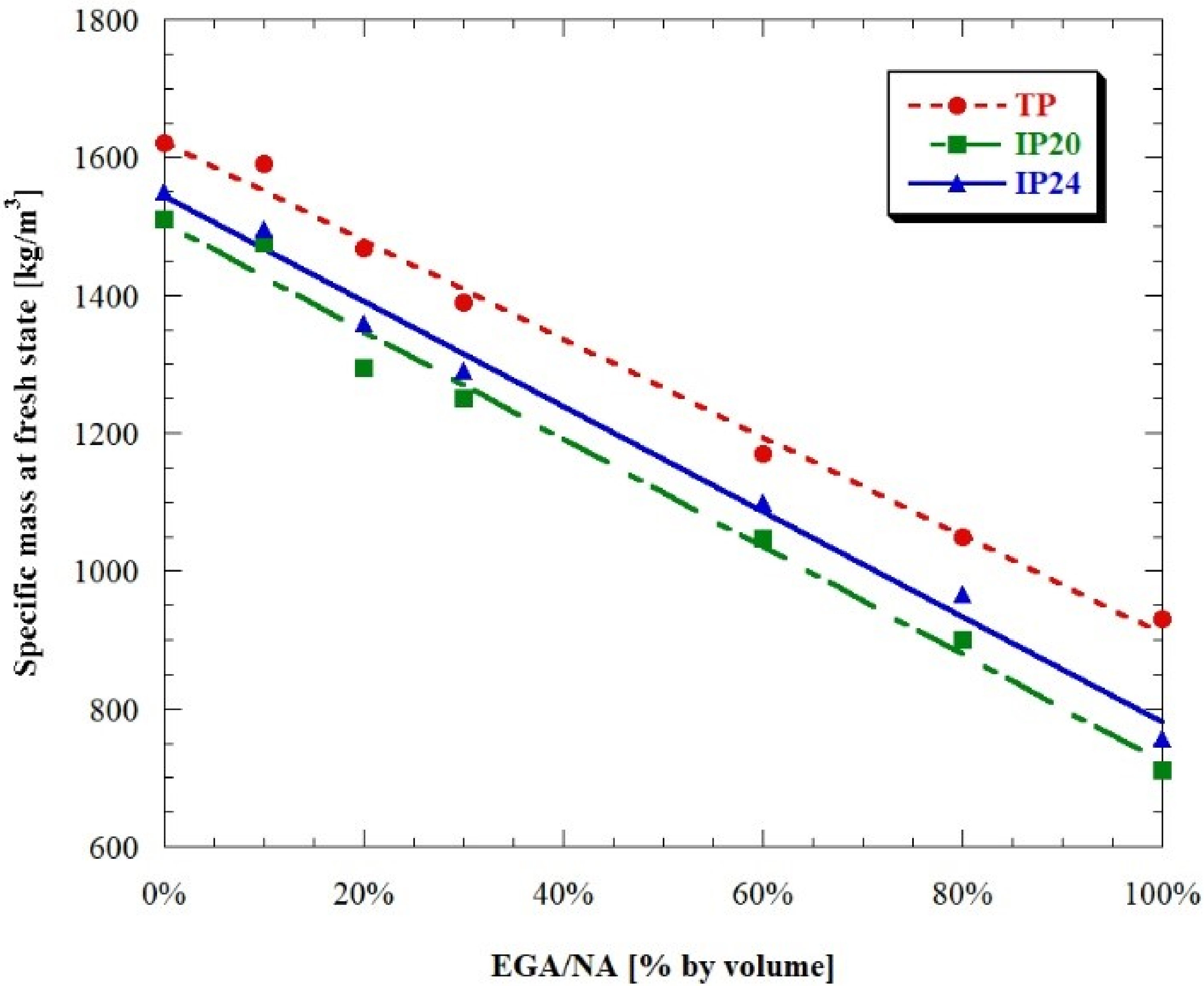

1800
1600
1400
1200
1000
800
600
Specific mass at fresh state [kg/m³]
0%
20%
40%
60%
80%
100%
EGA/NA [% by volume]
TP
IP20
IP24

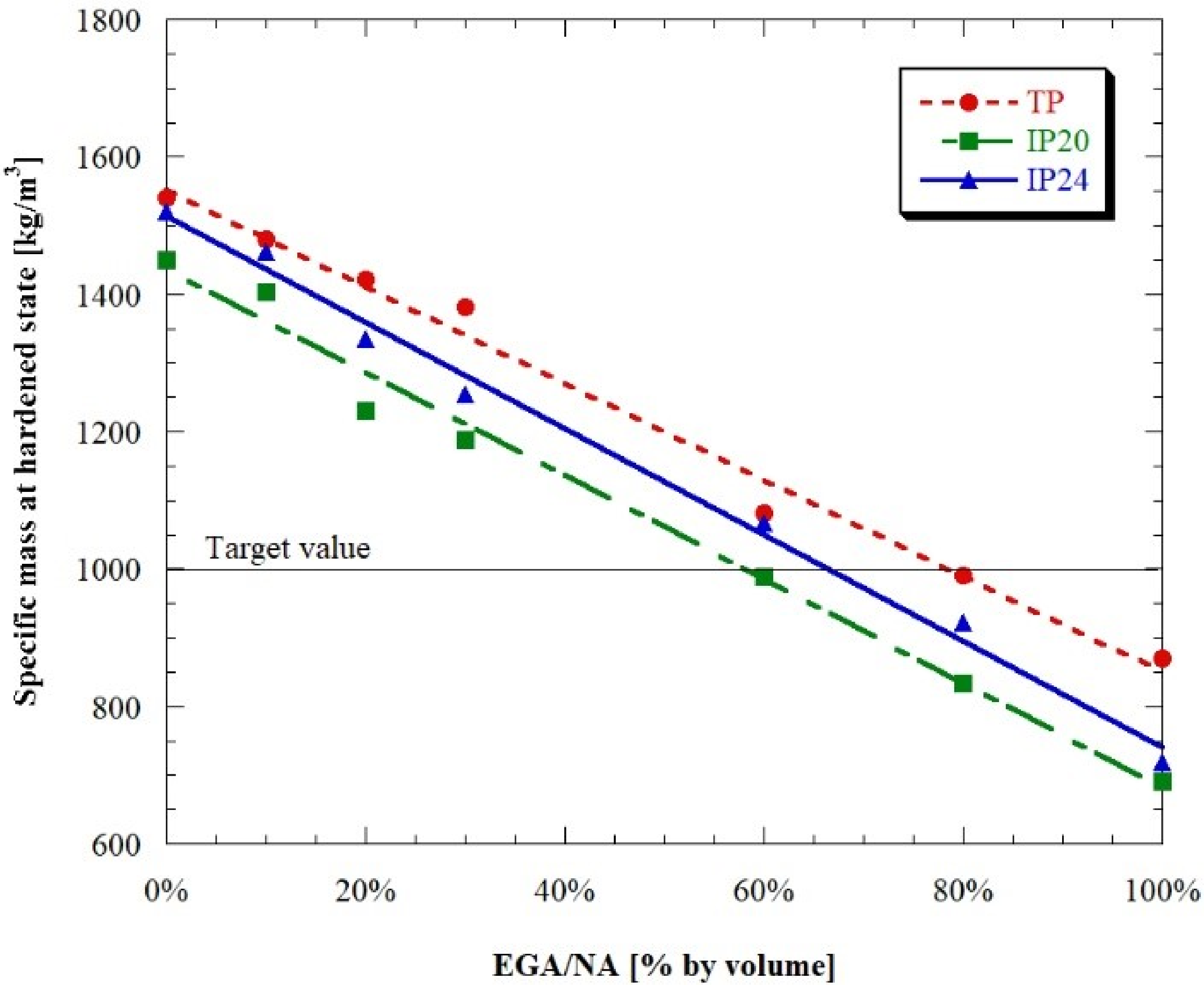

1800
1600
1400
1200
1000
800
600
Specific mass at hardened state [kg/m$^3$]
0%
20%
40%
60%
80%
100%
EGA/NA [% by volume]
TP
IP20
IP24
Target value

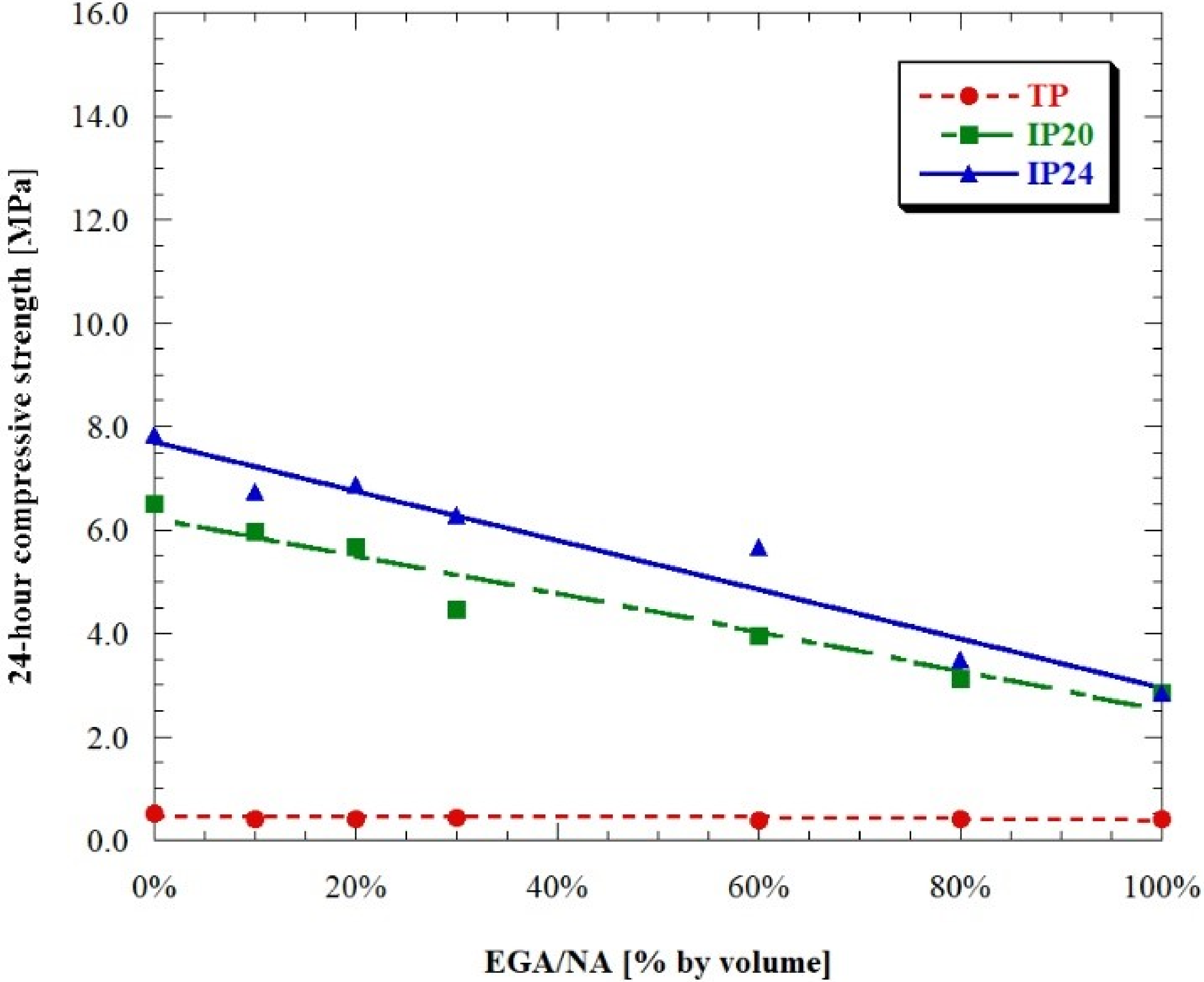

TP
IP20
IP24
24-hour compressive strength [MPa]
16.0
14.0
12.0
10.0
8.0
6.0
4.0
2.0
0.0
0%
20%
40%
60%
80%
100%
EGA/NA [% by volume]

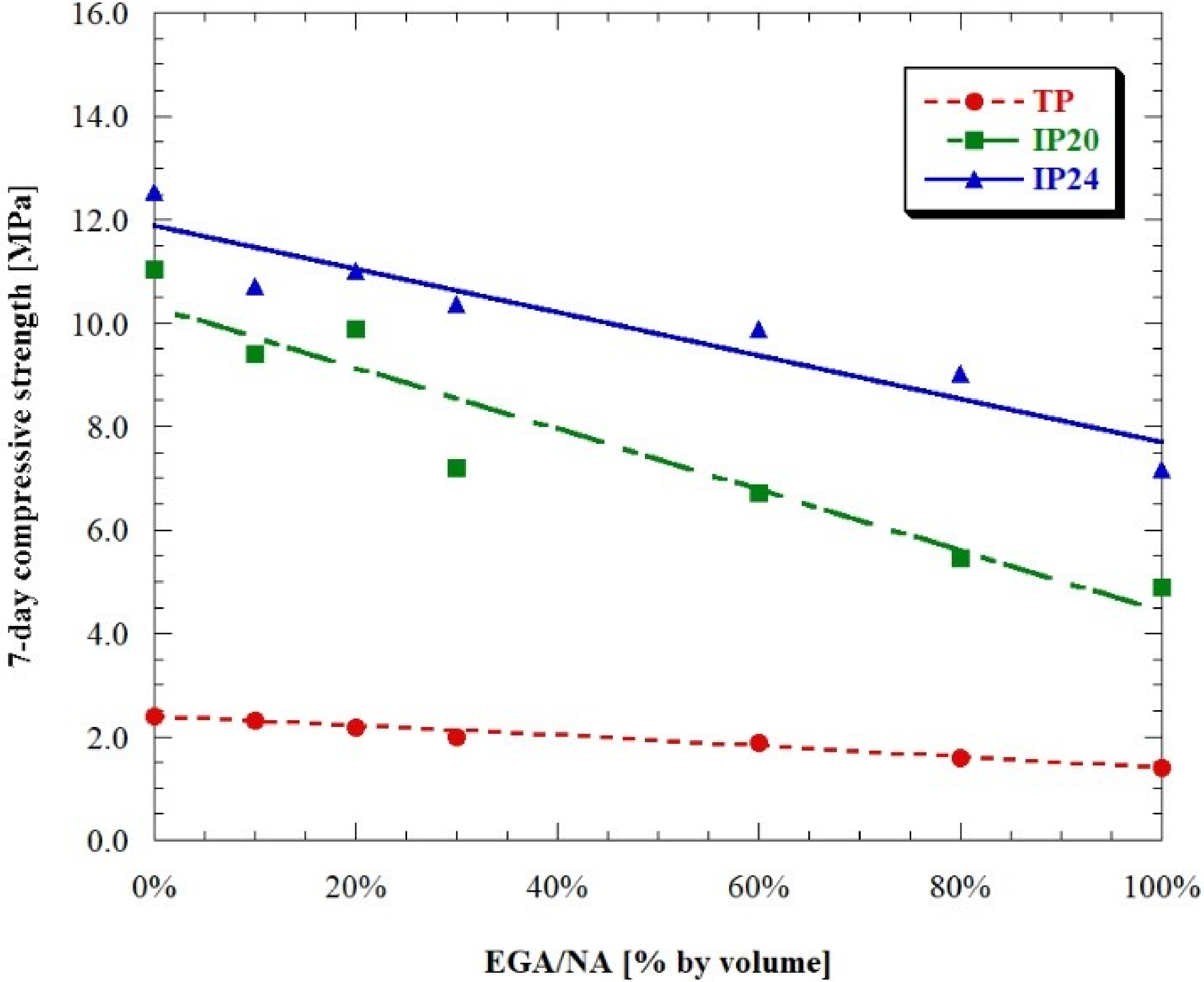
16.0
14.0
12.0
10.0
8.0
6.0
4.0
2.0
0.0
7-day compressive strength [MPa]
0%
20%
40%
60%
80%
100%
EGA/NA [% by volume]
TP
IP20
IP24

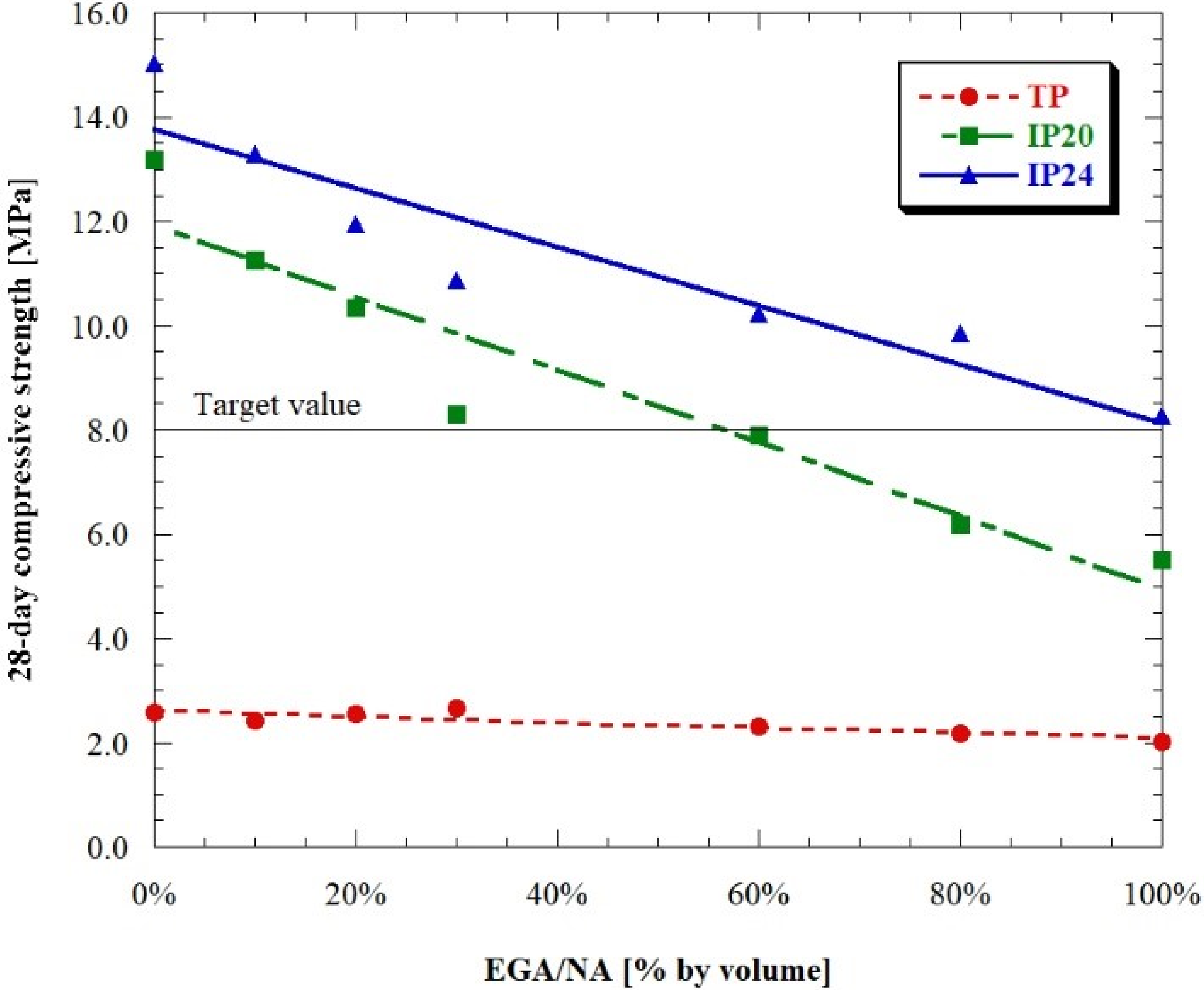

28-day compressive strength [MPa]
16.0
14.0
12.0
10.0
8.0
6.0
4.0
2.0
0.0
0%
20%
40%
60%
80%
100%
EGA/NA [% by volume]
TP
IP20
IP24
Target value

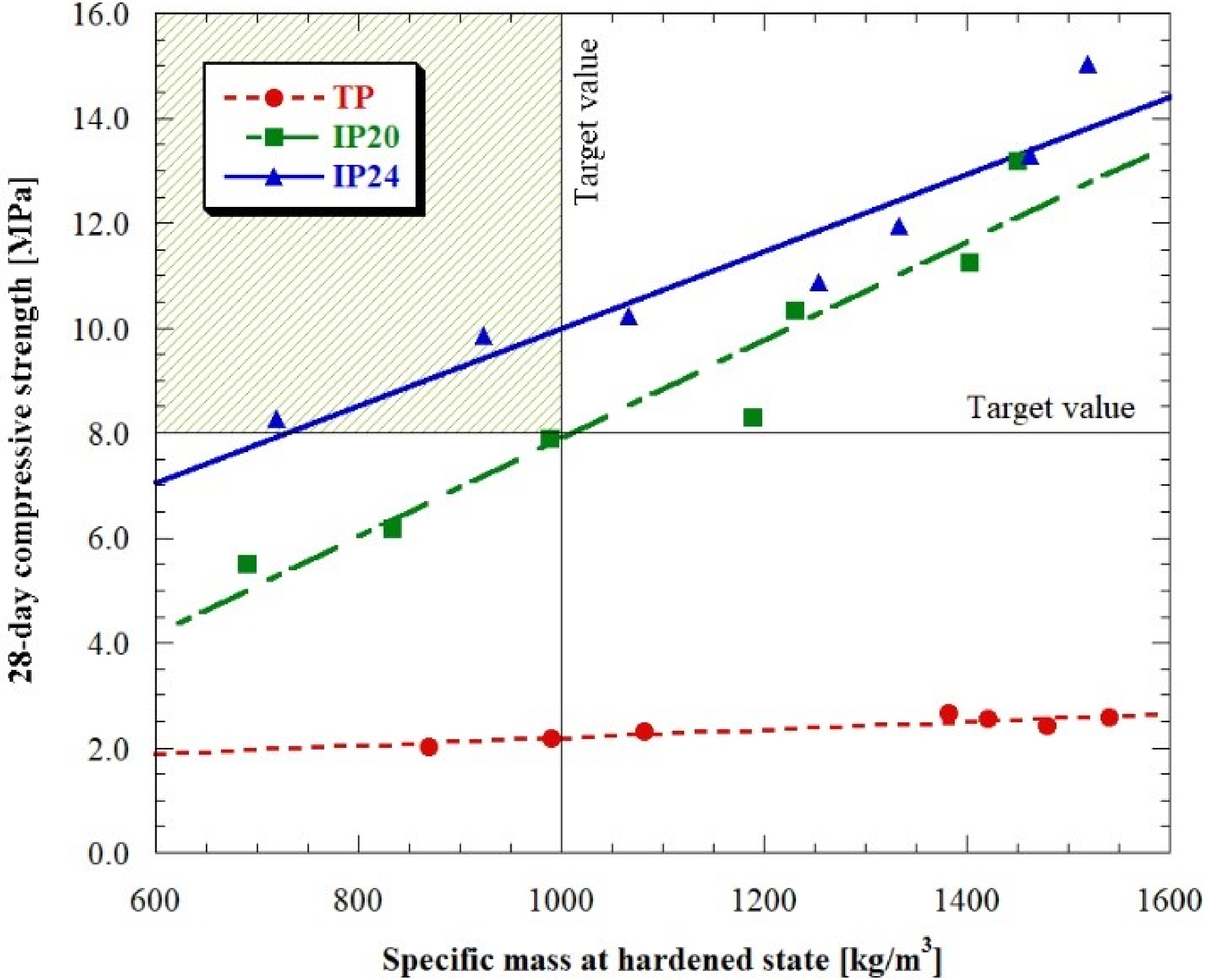

TP
IP20
IP24
Target value
Target value
28-day compressive strength [MPa]
Specific mass at hardened state [kg/m3]
0.0
2.0
4.0
6.0
8.0
10.0
12.0
14.0
16.0
600
800
1000
1200
1400
1600

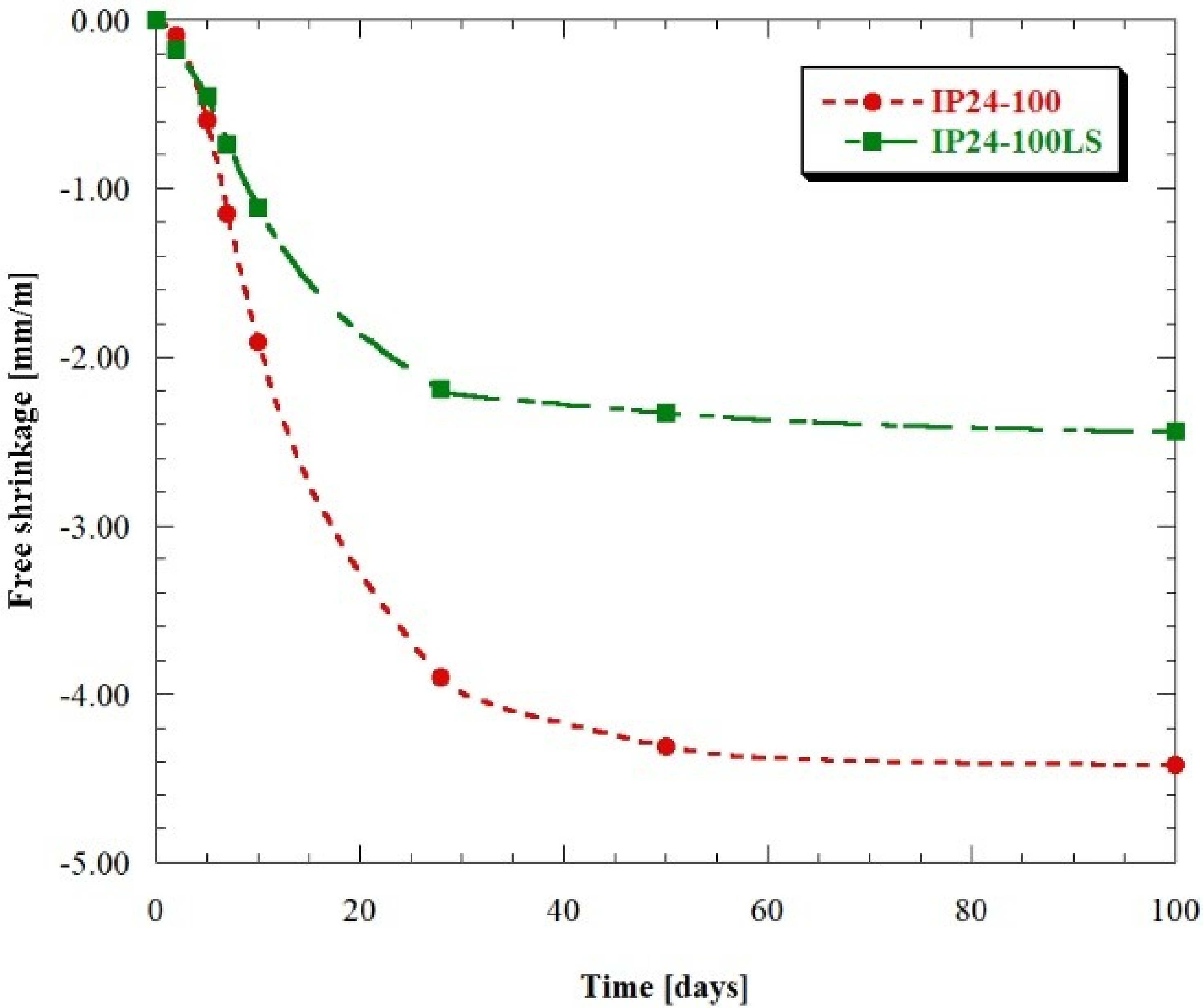

IP24-100
IP24-100LS
Free shrinkage [mm/m]
Time [days]
0.00
-1.00
-2.00
-3.00
-4.00
-5.00
0
20
40
60
80
100

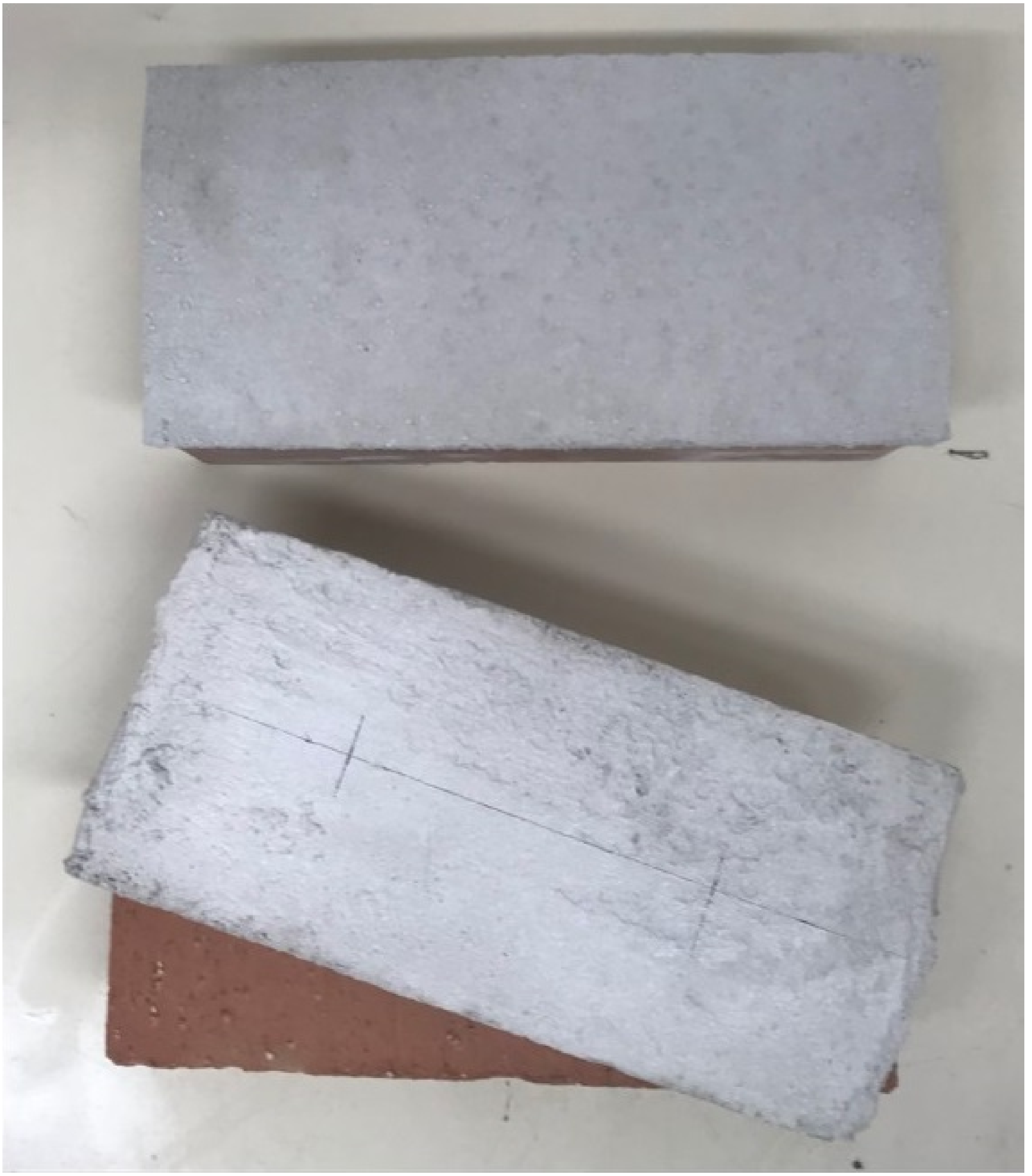



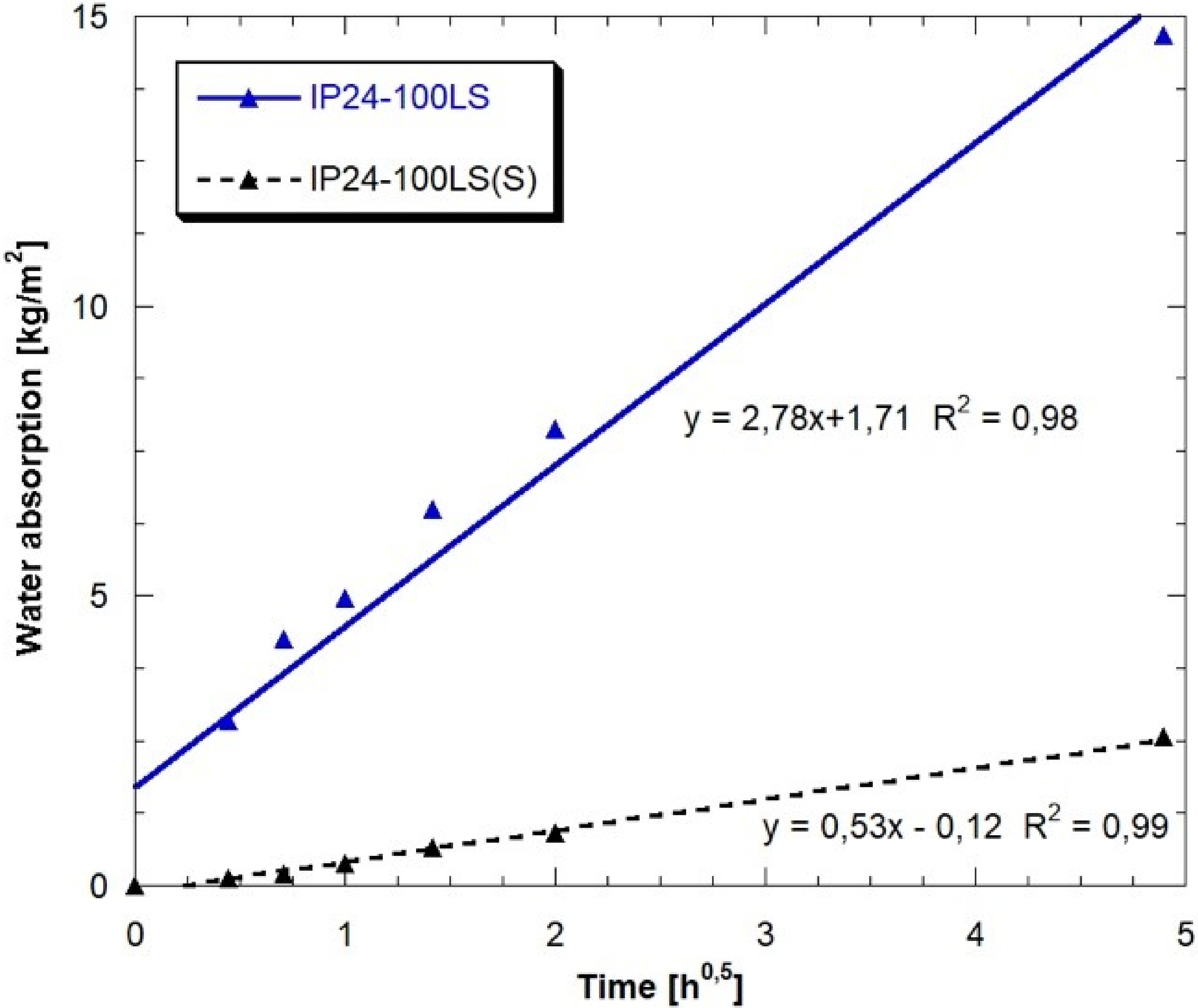

IP24-100LS
IP24-100LS(S)
y = 2,78x+1,71  R2 = 0,98
y = 0,53x - 0,12  R2 = 0,99
Water absorption [kg/m2]
Time [h0,5]
0
5
10
15
0
1
2
3
4
5

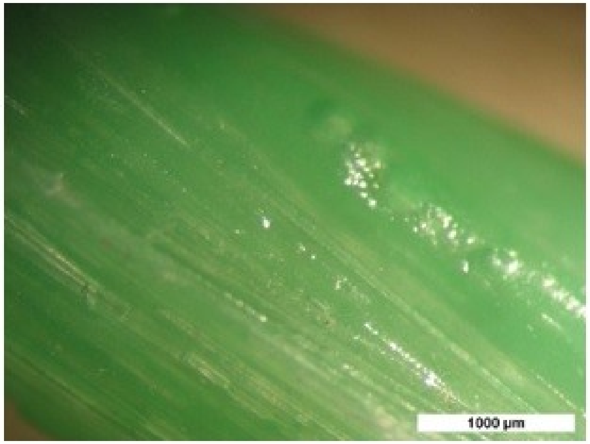
1000 µm


1000 µm

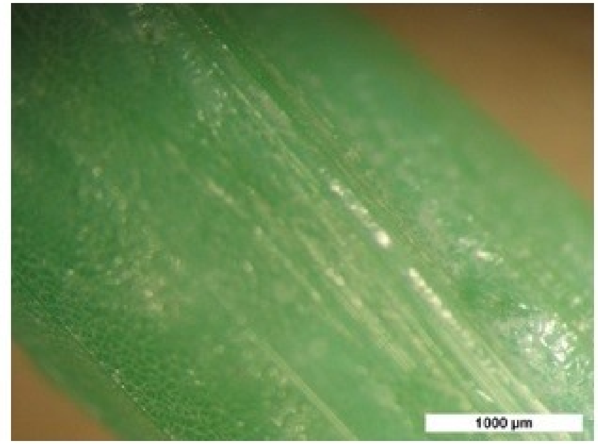
1000 µm